AoI-Driven Statistical Delay and Error-Rate Bounded QoS Provisioning for mURLLC Over UAV-Multimedia 6G Mobile Networks Using FBC

Xi Zhang, *Fellow, IEEE*, Jingqing Wang, and H. Vincent Poor, *Life Fellow, IEEE*

***Abstract*— Massive ultra-reliable and low latency communications (mURLLC) has emerged as new and dominating 6G-standard services to support statistical quality-of-services (QoS) provisioning for delay-sensitive data transmissions. To measure the freshness of updated information, age of information (AoI) has recently formed as the new dimension of QoS metric. Since status updates usually consist of a small number of information bits but warrant ultra-low latency, integrating AoI with *finite blocklength coding* (FBC) creates an alternative promising solution for mURLLC. On the other hand, to solve the massive connectivity issues imposed by mURLLC, *unmanned aerial vehicle* (UAV) has been developed to significantly enhance the line-of-sight (LOS) coverage while guaranteeing various QoS requirements. However, how to efficiently integrate the above new techniques for statistical delay and error-rate bounded QoS provisioning in UAV systems has been neither well understood nor thoroughly studied. To overcome these challenges, we propose FBC based statistical delay and error-rate bounded QoS provisioning schemes which leverage AoI as a key QoS provisioning technique for mURLLC over UAV mobile networks. First, we develop FBC based UAV system models. Second, we build up AoI-metric based modeling frameworks to upper-bound peak AoI violation probability using FBC. Third, we formulate and solve FBC based peak AoI violation probability minimization problem. Forth, we jointly optimize peak AoI violation probability and ϵ-effective capacity and characterize their tradeoffs. Finally, our simulations validate and evaluate our developed schemes.**

***Index Terms*— Statistical delay and error-rate bounded QoS, peak AoI violation probability, UAV, 6G mURLLC, FBC.**

I. Introduction

THE delay-bounded quality-of-services (QoS) theory [1] [2] [3] and the stochastic network calculus (SNC) [4] have been proposed and developed to characterize queueing behaviors in supporting explosively growing demands of time-sensitive wireless multimedia applications over 5G and the upcoming 6G mobile networks which are defined and detailed in [5]–[7]. Due to the highly time-varying nature of wireless fading channels, researchers have proposed the concept of *statistical QoS provisioning* [8] [9], in terms of effective capacity [10] and delay-bound violation probabilities, in supporting delay-sensitive multimedia wireless services over multimedia mobile networks. The exponentially increasing volumes of bandwidth-intensive and delay-sensitive multimedia traffic under stringent QoS requirements has raised the dramatical demands for bounded end-to-end delay (< 1 ms), super-reliability ($> 99.99999\%$), and extra-high energy efficiency in the 6G era.

Towards this end, the *massive Ultra-Reliable Low-Latency Communications* (mURLLC) [5], [11]–[15], as one of the 6G standard traffic services, have been proposed to quantitatively design and evaluate various QoS performances under stringent delay and error-rate bounded constraints. On the other hand, researchers have proposed and investigated the small-packet data communication techniques, such as finite blocklength coding (FBC) [16]–[19], in supporting various massive access techniques for reducing the access latency and decoding complexity at the receivers while guaranteeing stringent QoS requirements of 6G mURLLC for time-sensitive wireless services. The maximum achievable coding rate using FBC over Additive white Gaussian noise (AWGN) channels has been derived in [20]. However, although small-packet communications used in FBC-based wireless mobile networks are usually employed for massive access to reduce access latency and decoding complexity, how to upper-bound the decoding error probability while supporting 6G mURLLC is still a challenging research topic.

On the other hand, one of the major challenges for ensuring the stringent QoS requirements of 6G mURLLC is the massive connectivity and massive coverage issues imposed by the massive access. Most of the previous research works for 6G mURLLC have mainly focused on investigating the small-packet data transmissions between ground devices and ground base station (GBS). However, it is not always applicable to support reliable wireless accesses to a massive number of mobile devices while guaranteeing stringent 6G mURLLC requirements through the non-line-of-sight (NLOS) wireless links on the ground. Therefore, inspired by the advantages of deployment capability and high mobility, the *unmanned aerial vehicle* (UAV) and its associated IoU (Internet of UAV)

Manuscript received October 28, 2020; revised February 21, 2021; accepted April 11, 2021. Date of publication July 15, 2021; date of current version October 18, 2021. The work of Xi Zhang and Jingqing Wang was supported in part by the U.S. National Science Foundation under Grants: CCF-2008975, ECCS-1408601, and CNS-1205726; and in part by the U.S. Air Force under Grant FA9453-15-C-0423. The work of H. Vincent Poor was supported in part by the U.S. National Science Foundation under Grants: CCF-0939370 and CCF-1908308. *(Corresponding author: Xi Zhang.)*

Xi Zhang and Jingqing Wang are with the Networking and Information Systems Laboratory, Department of Electrical and Computer Engineering, Texas A&M University, College Station, TX 77843 USA (e-mail: xizhang@ece.tamu.edu; wang12078@tamu.edu).

H. Vincent Poor is with Department of Electrical and Computer Engineering, Princeton University, Princeton, NJ 08544 USA (e-mail: poor@princeton.edu).

Color versions of one or more figures in this article are available at https://doi.org/10.1109/JSAC.2021.3088625.

Digital Object Identifier 10.1109/JSAC.2021.3088625

systems [21], [22] have been proposed to potentially support various massive access techniques, including massive sensing, massive tracking, massive coverage, etc., by significantly enhancing the line-of-sight (LOS) coverage while guaranteeing various QoS requirements. In addition, the UAV systems have been widely recognized as an effective solution in supporting time-sensitive wireless services, such as real-time data-sensing and data-transmission applications, for URLLC to upper-bound both delay and error-rate [23]–[26]. The authors of [27] have establish a framework for enabling URLLC in the control and non-payload communications links of UAV wireless communication systems. The authors of [28] have proposed a UAV relay communication system in supporting URLLC and jointly optimized the UAV location and power to minimize decoding error probability while guaranteeing the latency constraints. The authors of [29] have studied the average packet error probability and effective throughput of the control link in UAV communications for URLLC. However, how to characterize mURLLC-enabled UAV communication schemes is still an open problem.

In addition, since the wireless data to be sensed and collected by the UAVs often changes rapidly, it is crucially important to measure and improve the performance of data freshness for real-time UAV sensing and transmissions, especially for a massive number of mobile devices for 6G mURLLC services. As a result, the concept of *age of information* (AoI) [30]–[32] has recently emerged as a new QoS matric to quantitatively characterize the freshness of information that a receiver has about the status of a remote data source, especially for the UAV applications, in supporting delay-sensitive/age-sensitive data fusions and transmissions. Since the status-updates normally consist only of a small number of information bits and need to be delivered to remote destinations as fast as possible, the design of small-packet communications are of great importance when considering the AoI metric over UAV wireless networks. Towards this end, FBC based AoI measurement has been proposed for UAV systems for maintaining the freshness of collected data by using small-packet data communications. However, how to efficiently integrate and implement the above new techniques for statistical delay and error-rate bounded QoS provisioning over 6G mURLLC standards has been neither well understood nor thoroughly studied.

To measure the data freshness over UAV wireless networks, there is number of research works focusing on analyzing the AoI metric over UAV multimedia mobile networks. The authors of [33] have studied the AoI-oriented optimal trajectory planning problem in UAV wireless sensor networks. The authors of [34] have formulated and solved an optimization problem to jointly optimize the UAV's flight trajectory as well as energy and service time allocations for data packet transmissions. The joint sensing time, transmission time, UAV trajectory, and target scheduling optimization problems have been investigated in [35] to minimize the system AoI function. The authors of [36] have modeled and analyzed the benefits of channel coding on AoI over broadcast networks. The aforementioned previous studies on AoI-driven UAV wireless communications were mainly conducted under the assumption of infinite blocklength. However, to guarantee the stringent URLLC requirements between UAV and ground devices, the conventional infinite-blocklength schemes are no longer applicable. To tackle this problem, an FBC-based information theoretic channel coding model has been developed in [18] [20]. Due to the non-linear/non-convex characteristics of AoI-driven optimization problems, how to formulate and solve the optimization problems to maximize the effective capacity remains a major challenge in supporting statistical delay and error-rate bounded QoS provisioning for 6G mURLLC, especially when applying the 3D wireless-link channels over UAV wireless networks using FBC.

To effectively overcome the above challenges, in this paper we develop AoI-driven statistical delay and error-rate bounded QoS provisioning schemes which leverage AoI as a key delay-bounded QoS provisioning technique in supporting mURLLC over UAV 6G multimedia mobile networks in the finite blocklength regime. In particular, we develop UAV wireless networking models with 3D wireless-link channels using FBC. We also build up AoI-metric based modeling frameworks by applying the SNC to characterize the upper-bounded peak AoI violation probability in the finite blocklength regime. Taking into account the transmit power and UAV trajectory constraints, we formulate and solve the peak AoI violation probability minimization problem in the finite blocklength regime. In addition, we jointly optimize the peak AoI violation probability and ϵ-effective capacity and characterize their tradeoff in supporting statistical delay and error-rate bounded QoS provisioning for 6G mURLLC. Finally, we conduct a set of simulations which validate and evaluate our proposed AoI-driven UAV schemes in supporting 6G mURLLC services.

The rest of this paper is organized as follows: Section II establishes FBC based UAV wireless networking models with 3D wireless-link channels. Section III builds up AoI-metric based modeling frameworks for 6G mURLLC using FBC. Section IV formulates and solves the FBC based peak AoI violation probability minimization problem for our proposed AoI-driven UAV schemes subject to the transmit power and UAV trajectory constraints. Section V jointly optimizes the peak AoI violation probability and ϵ-effective capacity and characterizes their tradeoff in the finite blocklength regime. Section VI validates and evaluates the system performances for our proposed schemes. The paper concludes with Section VII.

II. The System Models

Consider an FBC based UAV wireless network architecture model, which consists of multiple UAVs indexed by $u \in \{1, \dots, U\}$, one GBS, and K mobile users (MUs) which have the mission for timely sensing and collecting data from K sensing-targets, respectively, to bypass the LOS-blockages between sensing-targets (i.e., MUs) and the GBS (caused by the existing buildings/constructions or other obstacles in LOS path, see examples shown in Fig. 1), or perform other cellular-network devices' functions within the wireless cell covered by a number of UAVs and one GBS, as shown in Fig. 1. We assume that mobile users are equipped with single antenna while the GBS is equipped with multiple antennas indexed by $\{1, \dots, G\}$. First, the multiple UAVs collect

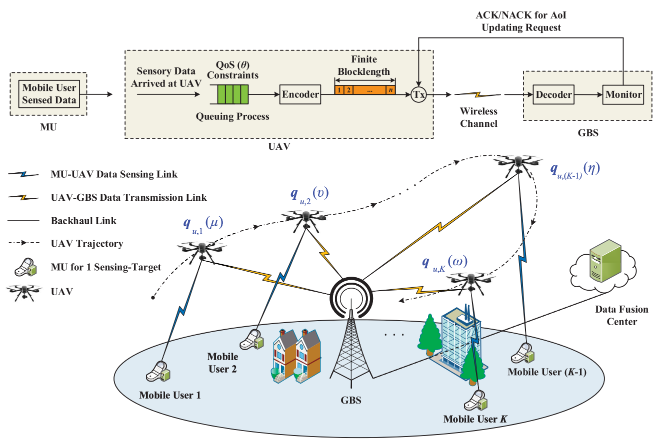

Fig. 1. The system architecture model for FBC based AoI-driven UAV multimedia mobile networks, where n is the codeword blocklength using FBC and $\boldsymbol{q}_{u,k}(\mu)$, $\boldsymbol{q}_{u,k}(\nu)$, $\boldsymbol{q}_{u,k}(\eta)$, and $\boldsymbol{q}_{u,k}(\omega)$ $(\mu,\nu,\eta,\omega \in \{1,\dots,N\})$ are the 3D-coordinates for the positions of UAV u with $u \in \{1,\dots,U\}$ when transmitting the μth status-update data packet, νth status-update data packet, ηth status-update data packet, and ωth status-update data packet, respectively, from mobile user (MU) k with $k \in \{1,\dots,K\}$. The kth mobile user (MU) monitors kth sensing-target with $k \in \{1,\dots,K\}$.

the sensed data from mobile devices distributed at different locations and then transmit the collected sensory data to the GBS for further processing before forwarding it to the data fusion center through the backhaul link. Since the data to be sensed and collected changes rapidly with time, all UAVs need to perform data sensing and transmitting for the sensing-targets frequently and repeatedly to maintain the freshness of the collected sensory data. We define each process that the multiple UAVs collect sensory data from mobile devices and transmit the data to the GBS as an update cycle. We consider the FBC-based UAV wireless network architecture model in which the nodes exchange *small packets*, typically with the packet size of $b \le 100$ bits, where b is the number of bits for each status-update data packet. From an information theoretic perspective, these status-update data packets are considered to be the data messages. Let $M = 2^b$ denote the cardinality of the message space. A message-encoder maps the message $m \in \{1,\dots,M\}$ into a codeword with a length of n channel uses, where n is also known as the number of channel uses in transmitting a data packet. We assume that time is slotted into frames each with a length of n channel uses. Therefore, we can derive the achievable coding rate as $b/n = (\log_2 M)/n$ in bits per channel use. Assume that there are N status-update cycles for each sensing-target k $(k = 1,\dots,K)$. In the μth status-update cycle $(\mu = 1,\dots,N)$, UAVs encode the μth status-update data packet into a codeword each with n channel uses and transmit the encoded data packet to the GBS.

In addition, assume that the locations of multiple UAVs and mobile users can be obtained in advance by using the Global Positioning System (GPS). Without loss of generality, we assume that the GBS is located at the coordinate-origin so that the 3D-coordinate for the position of the GBS is $\boldsymbol{q}_{\text{GBS}} = [0,0,0]$. Denote by $\boldsymbol{q}_{\text{G},k} = [x_{\text{G},k}, y_{\text{G},k}, 0]$ the 3D-coordinate for the position of mobile user/device k. The 3D-coordinate for the position of the uth UAV with $u \in \{1,\dots,U\}$ is denoted by $\boldsymbol{q}_{u,k}(\mu) = [x_{u,k}(\mu), y_{u,k}(\mu), z_{u,k}(\mu)]$ when transmitting the μth status-update data packet of sensing-target k with $\mu \in \{1,\dots,N\}$ and $H_{\min} \le z_{u,k}(\mu) \le H_{\max}$, where $H_{\min}$ and $H_{\max}$ represent the minimum and maximum flight altitudes of UAV u, respectively.

A. UAV-Based 3D Wireless Channel Model

We assume that the multiple UAVs indexed by $u \in \{1,\dots,U\}$ can choose to collect K targets along their flight trajectory. Define the binary variable $b_{u,k}(\mu)$ for *user association* between user k and UAV u when transmitting the μth status-update data packet as follows:

$$b_{u,k}(\mu) = \begin{cases} 1, & \text{if } k\text{th mobile user chooses to be connected} \\ & \text{to } u\text{th UAV for } \mu\text{th status-update packet;} \\ 0, & \text{otherwise.} \end{cases} \tag{1}$$

We assume that each UAV can be associated to multiple mobile users, however, each mobile user can only be associated with zero, or no more than one, UAV, i.e.,

$$\sum_{u=1}^{U} b_{u,k}(\mu) \le 1, \quad \forall k. \tag{2}$$

Denote by $\widetilde{\boldsymbol{q}}_{u,k}(\mu) = [x_{u,k}(\mu), y_{u,k}(\mu)]$ the trajectory of the uth UAV projected on the horizontal plane when transmitting the μth status-update data packet of sensing-target k. We can compute the distance, denoted by $d_{u,\text{GBS}}^{(k)}(\mu)$, between the uth UAV and the GBS when transmitting the μth status-update data packet obtained at sensing-target k as follows:

$$d_{u,\text{GBS}}^{(k)}(\mu) = \sqrt{\left\|\widetilde{\boldsymbol{q}}_{u,k}(\mu)\right\|^2 + \left[z_{u,k}(\mu)\right]^2} \tag{3}$$

where $\|\cdot\|$ is the Euclidean distance. In urban environments, the LOS link between any given UAV and ground nodes may be occasionally blocked by ground obstacles such as buildings. Similar to [37], the ground-to-UAV channel can be modeled as a weighted combination of two pathloss links: LOS and NLOS links, by taking into account their occurrence probabilities. We can derive the pathlosses, denoted by $PL_{u,\text{LOS}}^{(k)}$ and $PL_{u,\text{NLOS}}^{(k)}$, from the uth UAV to the GBS for transmitting the μth status-update data packet for sensing-target k for LOS and NLOS links, respectively, as follows:

$$\begin{cases} PL_{u,\text{LOS}}^{(k)} = \zeta_{\text{LOS}} \left(\dfrac{4\pi d_{u,\text{GBS}}^{(k)}(\mu)}{\lambda_0}\right)^2; \\ PL_{u,\text{NLOS}}^{(k)} = \zeta_{\text{NLOS}} \left(\dfrac{4\pi d_{u,\text{GBS}}^{(k)}(\mu)}{\lambda_0}\right)^2, \end{cases} \tag{4}$$

where $d_{u,\text{GBS}}^{(k)}(\mu)$ is given by Eq. (3), λ_0 is the system wavelength, and ζ_{LOS} and ζ_{NLOS} are the mean values of the excessive pathlosses of LOS and NLOS links, respectively. Based on the elevation angle-dependent probabilistic LOS model [37], the LOS probability, denoted by $p_{u,\mathrm{LOS}}^{(k)}$, is given as follows:

$$p_{u,\mathrm{LOS}}^{(k)} = \frac{1}{1+v_1 \exp\left[-v_2\left(\alpha_u^{(k)} - v1\right)\right]} \tag{5}$$

where v_1 and v_2 are the positive constants that depend on the environment and $\alpha_u^{(k)}$ is the elevation angle. Then, the NLOS probability is given as $p_{u,\mathrm{NLOS}}^{(k)} = 1 - p_{u,\mathrm{LOS}}^{(k)}$. Thus, the total pathloss, denoted by $PL_{u,\mathrm{LOS}}^{(k)}$ from the uth UAV to the GBS for transmitting the μth status-update data packet of sensing-target k is derived as follows:

$$PL_u^{(k)} = p_{u,\mathrm{LOS}}^{(k)} PL_{u,\mathrm{LOS}}^{(k)} + (1-p_{u,\mathrm{LOS}}^{(k)}) PL_{u,\mathrm{NLOS}}^{(k)}. \tag{6}$$

Given the location of the uth UAV, the received power, denoted by $P_{u,k}^{\mathsf{R}}(\mu)$, at the GBS for transmitting the μth status-update data packet of sensing-target k from the uth UAV is given as follows:

$$\begin{aligned} P_{u,k}^{\mathsf{R}}(\mu) &= \frac{\mathcal{P}_{u,k}^{(\mu)} G_{u,k}^{\mathrm{T}} G_{u,k}^{\mathrm{R}} \left[\widetilde{g}_{u,k}(\mu)\right]^2}{PL_{u,\mathrm{LOS}}^{(k)}} \\ &= \frac{\mathcal{P}_{u,k}^{(\mu)} G_{u,k}^{\mathrm{T}} G_{u,k}^{\mathrm{R}} [\widetilde{g}_{u,k}(\mu)\lambda_0]^2}{\left[4\pi d_{u,\mathrm{GBS}}^{(k)}(\mu)\right]^2 \left[p_{u,\mathrm{LOS}}^{(k)}\zeta_{u,\mathrm{LOS}}^{(k)} + (1-p_{u,\mathrm{LOS}}^{(k)})\zeta_{u,\mathrm{NLOS}}^{(k)}\right]} \end{aligned} \tag{7}$$

where $\mathcal{P}_{u,k}^{(\mu)}$ denotes the transmit power at the uth UAV for transmitting the μth status-update data packet of sensing-target k, $G_{u,k}^{\mathrm{T}}$ and $G_{u,k}^{\mathrm{R}}$ are the transmit and receive antenna gains, respectively, and $\widetilde{g}_{u,k}(\mu)$ is a complex random variable with $\mathbb{E}\left[|\widetilde{g}_{u,k}(\mu)|^2\right] = 1$, which represents the small-scale fading due to multi-path propagation, where $\mathbb{E}[\cdot]$ is the expectation operation. The above Eq. (7) shows that the received power $P_{u,k}^{\mathsf{R}}(\mu)$ depends on the transmit antenna gain, the receive antenna gain, and the large-scale channel power, i.e., pathloss. Specifically, for directional transmission with either fixed antenna pattern or flexible beamforming, the relative position between the uth UAV and the GBS determines the azimuth angles of departure (AoDs) and azimuth angles of arrival (AoAs) of the signal propagation, which thus affects the transmit and receive antenna gains.

We can then derive the SNR, denoted by $\gamma_{u,k}^{(\mu)}$, for transmitting the μth status-update data packet collected at sensing-target k from the uth UAV to the GBS as follows:

$$\begin{aligned} \gamma_{u,k}^{(\mu)} &= b_{u,k}(\mu)\mathcal{P}_{u,k}^{(\mu)} G_{u,k}^{\mathrm{T}} G_{u,k}^{\mathrm{R}} [\widetilde{g}_{u,k}(\mu)\lambda_0]^2 \\ &\quad \times \Bigg\{ (4\pi\sigma)^2 \left\{ \left\|\widetilde{\boldsymbol{q}}_{u,k}(\mu)\right\|^2 + [z_{u,k}(\mu)]^2 \right\} \\ &\quad \times \left[p_{u,\mathrm{LOS}}^{(k)}\zeta_{u,\mathrm{LOS}}^{(k)} + (1-p_{u,\mathrm{LOS}}^{(k)})\zeta_{u,\mathrm{NLOS}}^{(k)}\right] \Bigg\}^{-1} \end{aligned} \tag{8}$$

where σ^2 is the noise power. Denote by $\mathsf{N} \triangleq \{1,\ldots,N\}$ and $\mathsf{U} \triangleq \{1,\ldots,U\}$ the index sets for all N status-update data packets and U UAVs with their cardinalities: $|\mathsf{N}| = N$ and $|\mathsf{U}| = U$, respectively. The flight trajectory, denoted by $\boldsymbol{Q}_u(\mu)$, of UAV u for transmitting the μth status-update data packet ($\mu \in \mathsf{N}$) from mobile user 1 to mobile user K can be characterized as in the following sequence:

$$\boldsymbol{Q}_u(\mu) \triangleq \left\{\boldsymbol{q}_{u,1}(\mu), \ldots, \boldsymbol{q}_{u,K}(\mu)\right\}. \tag{9}$$

Denote by $\mathsf{K} \triangleq \{1,\ldots,K\}$ the index set for all K sensing-targets with $|\mathsf{K}| = K$. Then, the trajectory of UAV u $(u = 1,\ldots,U)$ for sensing-target $k \in \mathsf{K}$ is specified by the following constraints:

$$\begin{cases} \left\|\boldsymbol{q}_{u,k}(\mu+1) - \boldsymbol{q}_{u,k}(\mu)\right\| \le V_{\max} T_{u,k}(\mu), \\ \qquad\qquad \mu = 1,\ldots,(N-1), k \in \mathsf{K}; & (10) \\ \left\|\boldsymbol{q}_{u,k}(\mu) - \boldsymbol{q}_{u',k}(\nu)\right\|^2 \ge d_{\min},\ \mu,\nu \in \mathsf{N}, k \in \mathsf{K}; & (11) \\ \boldsymbol{q}_{u,1}(\mu) = \boldsymbol{q}_{u,\mathrm{I}}; & (12) \\ \boldsymbol{q}_{u,(K+1)}(\mu) = \boldsymbol{q}_{u,\mathrm{F}}; & (13) \\ H_{\min} \le z_{u,k}(\mu) \le H_{\max}, & (14) \end{cases}$$

where $T_{u,k}(\mu)$ is the total sojourn time for transmitting the μth status-update data packet of sensing-target k from UAV u to the GBS, $V_{\max}$ is the maximum allowable velocity of UAVs, $d_{\min}$ is the minimum inter-UAV distance between UAV u and u' ($u \neq u'$ and $u, u' \in \mathsf{U}$) to ensure no collision, and $\boldsymbol{q}_{u,\mathrm{I}}$ and $\boldsymbol{q}_{u,\mathrm{F}}$ denote the predetermined initial and final locations of UAV u, respectively. The constraint in Eq. (10) implies that the UAV trajectory is limited by the maximum allowable velocity $V_{\max}$ for transmitting one status-update data packet of each sensing-target during each status-update cycle. This indicates that the UAVs cannot move too fast when transmitting the status-update data packets during each status-update cycle. Eq. (11) ensures that the UAV trajectory is subject to collision avoidance constraints. The constraints in Eqs. (12) and (13) imply that each UAV has the initial and the final locations where the UAV must start from and arrive at during N status-update cycles. Eq. (14) guarantees that the flight altitude of each UAV is constrained by both the minimum and maximum flight altitudes.

B. The Channel Coding Rate in the Finite Blocklength Regime

Definition 1 (The (n, M, ϵ)-Code): We define a message set $\mathcal{M} = \{1,\ldots,M\}$ and a message m is uniformly distributed on $\mathcal{M}$, where M is the number of codewords and ϵ is the decoding error probability. Correspondingly, we define an (n, M, ϵ)-code as follows:

- An encoder Υ: $\{1,\ldots,M\} \mapsto \mathcal{A}^n$ that maps the message $m \in \{1,\ldots,M\}$ into a codeword, denoted by $\boldsymbol{x^{(n)}}$, with length n, where $\mathcal{A}^n$ is the codebook which represents the set of all the possible codewords mapped by the encoding function Υ.
- A decoder $\mathcal{D}$: $\mathcal{B}^n \mapsto \{1,\ldots,M\}$ that decodes the received message into $\widehat{m}$, where $\mathcal{B}^n$ is the set of received codewords of length n and $\widehat{m}$ denotes the estimated signal received at the receiver. The decoder $\mathcal{D}$ need to satisfy the following maximum error probability constraint:

$$\Pr\{\widehat{m} \neq m\} \le \epsilon. \tag{15}$$

Definition 2 (The Channel Coding Rate): Traditionally, Shannon's second theorem generally requires infinite blocklength for attaining the accurate approximation of maximum coding rate. However, as noted above, Shannon's capacity formula cannot be applied when considering the limited bandwidth and *stringent delay-bounded QoS requirements* in supporting 6G mURLLC services in the finite block-length regime. Therefore, we consider an alternative solution by providing the *statistical* delay and error-rate bounded QoS guarantees through applying the finite blocklength coding (FBC) technique [15] [16] [17], where 6G mURLLC services can be *statistically* guaranteed with the controlled small violation probabilities. Using [16] [17], the *maximum achievable coding rate*, denoted by $R\left(\gamma_{u,k}^{(\mu)}\right)$, in bits per channel use with coding blocklength n for transmitting the μth status-update data packet of sensing-target k from UAV u to the GBS in the finite blocklength regime can be derived as follows [16] [17]:

$$R\left(\gamma_{u,k}^{(\mu)}\right) = C_{\epsilon}\left(\gamma_{u,k}^{(\mu)}\right) + \mathcal{O}\left(\frac{\log n}{n}\right) \tag{16}$$

where $C_{\epsilon}\left(\gamma_{u,k}^{(\mu)}\right)$ is the *outage capacity* derived in [16] and $\mathcal{O}(\cdot)$ is the big O notation. The above Eq. (16) implies that the maximum achievable coding rate converges quickly to the outage capacity $C_{\epsilon}\left(\gamma_{u,k}^{(\mu)}\right)$ as the codeword blocklength n tends to infinity.

For our proposed UAV-based model, we assume that each status-update data packet μ contains fixed $\log_2(M) = b$ bits of information. Thus, we obtain a fixed channel coding rate $R\left(\gamma_{u,k}^{(\mu)}\right) = (\log_2 M)/n$. Given a fixed channel coding rate, we can obtain the decoding error probability function, denoted by $\epsilon\left(\gamma_{u,k}^{(\mu)}\right)$, when transmitting the μth status-update data packet of sensing-target k $(k = 1, \ldots, K)$ from UAV u to the GBS as follows:

$$\epsilon\left(\gamma_{u,k}^{(\mu)}\right) \approx Q\left(\frac{C\left(\gamma_{u,k}^{(\mu)}\right) - \frac{\log_2 M}{n}}{\sqrt{V\left(\gamma_{u,k}^{(\mu)}\right)/n}}\right) \tag{17}$$

where $R\left(\gamma_{u,k}^{(\mu)}\right) = (\log_2 M)/n$ is the coding rate given by Eq. (16), $Q(\cdot)$ is the Q-function, and $C\left(\gamma_{u,k}^{(\mu)}\right)$ and $V\left(\gamma_{u,k}^{(\mu)}\right)$ are the *channel capacity* and *channel dispersion*, respectively, which are given in the following equations, respectively:

$$\begin{cases} C\left(\gamma_{u,k}^{(\mu)}\right) = \log_2\left(1 + \gamma_{u,k}^{(\mu)}\right); \\ V\left(\gamma_{u,k}^{(\mu)}\right) = 1 - \frac{1}{\left(1+\gamma_{u,k}^{(\mu)}\right)^2}. \end{cases} \tag{18}$$

III. UAV-Based Peak AoI Violation Portability Analyses for 6G mURLLC in the Finite Blocklength Regime

Since the collected sensory data at the UAV changes rapidly with time, it is crucially important to measure the performance of data freshness, i.e., AoI, for real-time UAV sensing and transmissions in the finite blocklength regime. In this section, we focus on characterizing the AoI metrics of the UAV-GBS link. We apply the SNC to characterize the upper-bounded peak AoI violation probability for our proposed AoI-driven UAV schemes in the finite blocklength regime for the given

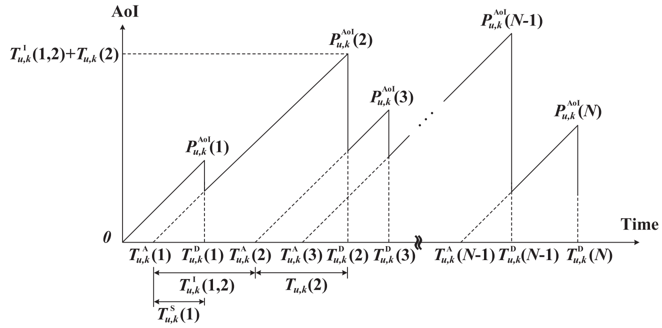

Fig. 2. The AoI evolution as a function of time for N finite-blocklength status-update data packets at the destination.

non-vanishing decoding error probability $\epsilon\left(\gamma_{u,k}^{(\mu)}\right)$, which is specified by Eq. (17).

A. AoI Metric Modelling

In order to measure and control the freshness of information, we adopt the concept of AoI as the performance metric to describe the freshness of the decoded data at the receiver of the GBS. As shown in Fig. 2, we denote by $T_{u,k}^{\mathrm{A}}(\mu)$, $T_{u,k}^{\mathrm{S}}(\mu)$, and $T_{u,k}^{\mathrm{D}}(\mu)$ $(\mu \in \mathsf{N},\ k \in \mathsf{K})$ the arrival time, service time, and departure time of the μth finite-blocklength status-update data packet for sensing-target k at UAV u, respectively. The service time $T_{u,k}^{\mathrm{S}}(\mu)$ is defined as the time required to process and transmit the μth finite-blocklength status-update data packet for sensing-target k from UAV u to the GBS. Without loss of generality, we set $T_{u,k}^{\mathrm{A}}(0) = 0$. We apply a Bernoulli process to model the stochastic arrivals of each packet at the UAVs. When UAVs perform video-based data sensing such as precision agriculture, the successful sensing probability satisfies the sensing model introduced in [35], [38], and [39]. In particular, the μth status-update data packet of sensing-target k arrives at UAV u with the arrival probability, denoted by $p_{u,k}(\mu)$, which is given by [35]:

$$p_{u,k}(\mu) = e^{-\xi d_{u,k}(\mu)} \tag{19}$$

where ξ is the sensing performance parameter and $d_{u,k}(\mu)$ is the distance between UAV u and mobile user/device k, which is given as follows:

$$d_{u,k}(\mu) = \left\|\boldsymbol{q}_{u,k}(\mu) - \boldsymbol{q}_{\mathrm{G},k}\right\|. \tag{20}$$

We set a successful arrival probability threshold, denoted by p_{th}, for the UAVs, i.e., $p_{u,k}(\mu) \geq p_{\mathrm{th}}$. As shown in Fig. 2, we define $T_{u,k}^{\mathrm{I}}(\nu,\mu) \triangleq T_{u,k}^{\mathrm{A}}(\mu) - T_{u,k}^{\mathrm{A}}(\nu)$ as the inter-arrival time between the νth status-update data packet and the μth status-update data packet of sensing-target k for $1 \leq \nu \leq \mu$. Then, $T_{u,k}^{\mathrm{I}}(\mu-1,\mu)$ represents the inter-arrival time between the $(\mu-1)$th and the μth status-update data packets of sensing-target k. Then, the inter-arrival time $T_{u,k}^{\mathrm{I}}(\nu,\mu)$ between the νth status-update data packet and the μth status-update data packet of sensing-target k for $1 \leq \nu \leq \mu$ can be rewritten as follows:

$$T_{u,k}^{\mathrm{I}}(\nu,\mu) = \sum_{j=\nu+1}^{\mu} T_{u,k}^{\mathrm{I}}(j-1,j). \tag{21}$$

The cumulative service time, denoted by $T^{\mathrm{S}}_{u,k}(\nu,\mu)$, for the νth status-update data packet up to and including the μth status-update data packet of sensing-target k can be derived as follows:

$$T^{\mathrm{S}}_{u,k}(\nu,\mu) = \sum_{j=\nu}^{\mu} T^{\mathrm{S}}_{u,k}(j). \tag{22}$$

Considering an FCFS queue, we can derive the departure time $T^{\mathrm{D}}_{u,k}(\mu)$ $(\mu \geq 1)$ for μ status-update data packets of sensing-target k as follows [40]:

$$T^{\mathrm{D}}_{u,k}(\mu) = \max_{\nu\in\mathsf{N},\nu\leq\mu} \left\{T^{\mathrm{A}}_{u,k}(\nu) + T^{\mathrm{S}}_{u,k}(\nu,\mu)\right\}. \tag{23}$$

In addition, we can derive the total sojourn time, denoted by $T_{u,k}(\mu)$, for the μth status-update data packet of sensing-target k as follows:

$$\begin{aligned} T_{u,k}(\mu) &\triangleq T^{\mathrm{D}}_{u,k}(\mu) - T^{\mathrm{A}}_{u,k}(\mu) \\ &= \max_{\nu\in\mathsf{N},\nu\leq\mu} \left\{T^{\mathrm{S}}_{u,k}(\nu,\mu) - T^{\mathrm{I}}_{u,k}(\nu,\mu)\right\}. \end{aligned} \tag{24}$$

Observing from Fig. 2, we can derive the peak AoI, denoted by $P^{\mathrm{AoI}}_{u,k}(\mu)$, for the μth status-update data packet of sensing-target k at UAV u in the finite blocklength regime as follows:

$$P^{\mathrm{AoI}}_{u,k}(\mu) = T^{\mathrm{D}}_{u,k}(\mu) - T^{\mathrm{A}}_{u,k}(\mu-1). \tag{25}$$

Then, using Eqs. (21), (24), and (25), the peak AoI $P^{\mathrm{AoI}}_{u,k}(\mu)$ for the μth status-update data packet of sensing-target k can be rewritten as follows:

$$P^{\mathrm{AoI}}_{u,k}(\mu) = T^{\mathrm{I}}_{u,k}(\mu-1,\mu) + T_{u,k}(\mu). \tag{26}$$

B. The Upper Bound on the Peak AoI Violation Probability in the Finite Blocklength Regime

To derive the upper bound on the peak AoI violation probability in the finite blocklength regime, we propose to apply the SNC to convert the random arrival and service times into the exponential domain [41]. By taking the exponential of the inter-arrival and service times, we can transform the inter-arrival and service times into the exponential domain by using the exponential functions, respectively, which are given as follows:

$$\begin{cases} \mathcal{T}^{\mathrm{I}}_{u,k}(\nu,\mu) \triangleq e^{T^{\mathrm{I}}_{u,k}(\nu,\mu)}; \\ \mathcal{T}^{\mathrm{S}}_{u,k}(\nu,\mu) \triangleq e^{T^{\mathrm{S}}_{u,k}(\nu,\mu)}. \end{cases} \tag{27}$$

Using Eq. (26), we can derive the peak AoI in the exponential domain $\mathcal{P}^{\mathrm{AoI}}_{u,k}(\mu)$ for the μth status-update data packet of sensing-target k as follows:

$$\mathcal{P}^{\mathrm{AoI}}_{u,k}(\mu) = e^{P^{\mathrm{AoI}}_{u,k}(\mu)} = \mathcal{T}^{\mathrm{I}}_{u,k}(\mu-1,\mu)\mathcal{T}_{u,k}(\mu) \tag{28}$$

where $\mathcal{T}^{\mathrm{I}}_{u,k}(\mu-1,\mu)$ and $\mathcal{T}_{u,k}(\mu)$ represent the inter-arrival time between the $(\mu-1)$th and μth status-update data packets of sensing-target k and total sojourn time for the μth status-update data packet of sensing-target k from UAV u to the GBS in the exponential domain, respectively, which are given as follows:

$$\begin{cases} \mathcal{T}^{\mathrm{I}}_{u,k}(\mu-1,\mu) = e^{T^{\mathrm{I}}_{u,k}(\mu-1,\mu)}; \\ \mathcal{T}_{u,k}(\mu) = e^{T_{u,k}(\mu)}. \end{cases} \tag{29}$$

Denote by A_{th} the peak AoI threshold in the number of channel uses for our proposed AoI-driven UAV schemes in the finite blocklength regime. The peak AoI violation probability is defined as the probability that the peak AoI $P^{\mathrm{AoI}}_{u,k}(\mu)$ exceeds a threshold A_{th}/n. Note that measuring the threshold a in channel uses rather than in frames allows us to assess the impact on the peak AoI violation probability of different choices of frame size. We can derive the peak AoI violation probability, denoted by $\epsilon^{(\mu,\mathrm{AoI})}_{u,k}$, for the μth status-update data packet of sensing-target k from UAV u to the GBS in the finite blocklength regime as follows:

$$\epsilon^{(\mu,\mathrm{AoI})}_{u,k} \triangleq \Pr\left\{P^{\mathrm{AoI}}_{u,k}(\mu) > \frac{A_{\text{th}}}{n}\right\}. \tag{30}$$

The peak AoI violation probability cannot be calculated directly. However, it can be upper-bounded by using the Mellin transform. Define the Mellin transform, denoted by $\mathcal{M}_{\mathcal{X}}(\theta)$, of a non-negative random variable $\mathcal{X}$ for $\theta > 0$ as follows:

$$\mathcal{M}_{\mathcal{X}}(\theta) \triangleq \mathbb{E}\left[\mathcal{X}^{(\theta-1)}\right] \tag{31}$$

where $\theta > 0$ is a free parameter which will be formally defined in Eq. (93) later. We can derive the Mellin transform of the peak AoI, denoted by $\mathcal{M}_{\mathcal{P}^{\mathrm{AoI}}_{u,k}(\mu)}(\theta)$, from UAV u to the GBS in the exponential domain as follows:

$$\begin{aligned} \mathcal{M}_{\mathcal{P}^{\mathrm{AoI}}_{u,k}(\mu)}(\theta) &= \mathbb{E}\left[\left(\mathcal{P}^{\mathrm{AoI}}_{u,k}(\mu)\right)^{(\theta-1)}\right] \\ &\leq \mathbb{E}\left[e^{(\theta-1)T^{\mathrm{I}}_{u,k}(\mu-1,\mu)}\right]\mathbb{E}\left[e^{(\theta-1)T_{u,k}(\mu)}\right] \\ &= \mathcal{M}_{\mathcal{T}^{\mathrm{I}}_{u,k}(\mu-1,\mu)}(\theta)\mathcal{M}_{\mathcal{T}_{u,k}(\mu)}(\theta) \end{aligned} \tag{32}$$

where $\mathcal{M}_{\mathcal{T}^{\mathrm{I}}_{u,k}(\mu-1,\mu)}(\theta)$ represents the Mellin transform of the inter-arrival time between the $(\mu-1)$th and μth status-update data packets of sensing-target k in the exponential domain and $\mathcal{M}_{\mathcal{T}_{u,k}(\mu)}(\theta)$ is the Mellin transform of the sojourn time of the μth status-update data packet of sensing-target k in the exponential domain. Based on the Mellin transform, we derive the upper bound on the peak AoI violation probability $\epsilon^{(\mu,\mathrm{AoI})}_{u,k}$ as detailed in the following theorem.

Theorem 1: Given the peak AoI threshold A_{th}, the upper bound on the peak AoI violation probability $\epsilon^{(\mu,\mathrm{AoI})}_{u,k}$ for our proposed AoI-driven UAV schemes in the finite blocklength regime is given as follows:

$$\epsilon^{(\mu,\mathrm{AoI})}_{u,k} \leq e^{-\frac{\theta A_{\text{th}}}{n}}\mathcal{K}_{u,k}(\theta,\mu) \tag{33}$$

where

$$\begin{aligned} \mathcal{K}_{u,k}(\theta,\mu) \triangleq\ & \mathcal{M}_{\mathcal{T}^{\mathrm{I}}_{u,k}(\mu-1,\mu)}(1+\theta)\Bigg[\sum_{\nu=1}^{\mu}\mathcal{M}_{\mathcal{T}^{\mathrm{S}}_{u,k}(\nu,\mu)}(1+\theta) \\ & \times\mathcal{M}_{\mathcal{T}^{\mathrm{I}}_{u,k}(\nu,\mu)}(1-\theta)\Bigg]. \end{aligned} \tag{34}$$

Proof: Using the Chernoff's inequality, we can derive the upper bound on the peak AoI violation probability $\epsilon^{(\mu,\mathrm{AoI})}_{u,k}$ for the μth status-update data packet of sensing-target k as follows:

$$\begin{aligned} \epsilon^{(\mu,\mathrm{AoI})}_{u,k} &= \Pr\left\{\mathcal{P}^{\mathrm{AoI}}_{u,k}(\mu) > e^{\frac{A_{\text{th}}}{n}}\right\} \leq e^{-\frac{\theta A_{\text{th}}}{n}}\mathcal{M}_{\mathcal{P}^{\mathrm{AoI}}_{u,k}(\mu)}(1+\theta) \\ &\leq e^{-\frac{\theta A_{\text{th}}}{n}}\mathcal{M}_{\mathcal{T}^{\mathrm{I}}_{u,k}(\mu-1,\mu)}(1+\theta)\mathcal{M}_{\mathcal{T}_{u,k}(\mu)}(1+\theta). \end{aligned} \tag{35}$$

To obtain the upper-bounded peak AoI violation probability, first using Eq. (24), we can derive the Mellin transform of the sojourn time $\mathcal{M}_{\mathcal{T}_{u,k}(\mu)}(1+\theta)$ in the exponential domain as follows:

$$\begin{aligned}\mathcal{M}_{\mathcal{T}_{u,k}(\mu)}(1+\theta) &= \mathbb{E}\left[e^{\theta T_{u,k}(\mu)}\right]\\ &\leq \sum_{\nu=1}^{\mu}\mathbb{E}\left[e^{\theta T^{\mathrm{S}}_{u,k}(\nu,\mu)}\right]\mathbb{E}\left[e^{-\theta T^{\mathrm{I}}_{u,k}(\nu,\mu)}\right]\\ &= \sum_{\nu=1}^{\mu}\mathcal{M}_{\mathcal{T}^{\mathrm{S}}_{u,k}(\nu,\mu)}(1+\theta)\mathcal{M}_{\mathcal{T}^{\mathrm{I}}_{u,k}(\nu,\mu)}(1-\theta)\end{aligned} \tag{36}$$

where $\mathcal{M}_{\mathcal{T}^{\mathrm{S}}_{u,k}(\nu,\mu)}(\theta)$ is the Mellin transform of the cumulative service time for the νth status-update data packet up to and including the μth status-update data packet of sensing-target k in the exponential domain and $\mathcal{M}_{\mathcal{T}^{\mathrm{I}}_{u,k}(\nu,\mu)}(\theta)$ is the Mellin transform of the inter-arrival time between the νth and μth status-update data packets of sensing-target k in the exponential domain. Then, by plugging Eq. (36) back into Eq. (35), we have

$$\epsilon_{u,k}^{(\mu,\mathrm{AoI})} \leq e^{-\frac{\theta A_{\mathrm{th}}}{n}}\mathcal{M}_{\mathcal{T}^{\mathrm{I}}_{u,k}(\mu-1,\mu)}(1+\theta)\left[\sum_{\nu=1}^{\mu}\mathcal{M}_{\mathcal{T}^{\mathrm{S}}_{u,k}(\nu,\mu)}(1+\theta)\times\mathcal{M}_{\mathcal{T}^{\mathrm{I}}_{u,k}(\nu,\mu)}(1-\theta)\right]. \tag{37}$$

We define a kernel function, denoted by $\mathcal{K}_{u,k}(\theta,\mu)$, as follows:

$$\mathcal{K}_{u,k}(\theta,\mu) \triangleq \mathcal{M}_{\mathcal{T}^{\mathrm{I}}_{u,k}(\mu-1,\mu)}(1+\theta)\left[\sum_{\nu=1}^{\mu}\mathcal{M}_{\mathcal{T}^{\mathrm{S}}_{u,k}(\nu,\mu)}(1+\theta)\times\mathcal{M}_{\mathcal{T}^{\mathrm{I}}_{u,k}(\nu,\mu)}(1-\theta)\right]. \tag{38}$$

Thus, plugging Eq. (38) into Eq. (37), we can obtain Eq. (33), which completes the proof of Theorem 1. ■

Remarks on Theorem 1: While it is infeasible to derive the exact closed-form expression for the peak AoI violation probability $\epsilon_{u,k}^{(\mu,\mathrm{AoI})}$ for our proposed schemes in the finite blocklength regime, Theorem 1 yields the accurate upper-bound for the peak AoI violation probability derived in Eqs. (33) and (34), which provides with practically very useful designing guidance for engineering, modeling, and evaluating our proposed AoI-driven UAV multimedia mobile networks in the finite blocklength regime.

C. The Mellin Transform of the Inter-Arrival and Service Times

1) The Mellin Transform of the Inter-Arrival Time: Based on the $(\sigma^{\mathrm{I}}(\theta),\rho^{\mathrm{I}}(\theta))$-bounded process [40], the Mellin transform of the inter-arrival time in the exponential domain can be upper-bounded as follows:

$$\begin{aligned}\mathcal{M}_{\mathcal{T}^{\mathrm{I}}_{u,k}(\nu,\mu)}(1+\theta) &= \mathbb{E}\left[\left\{\mathcal{T}^{\mathrm{I}}_{u,k}(\nu,\mu)\right\}^{\theta}\right]\\ &\leq e^{\theta\left[(\mu-\nu)\rho^{\mathrm{I}}_{u,k}(\theta)+\sigma^{\mathrm{I}}_{u,k}(\theta)\right]}.\end{aligned} \tag{39}$$

Thus, setting $\nu=(\mu-1)$, we can derive the Mellin transform of the inter-arrival time between the $(\mu-1)$th and the μth status-update data packets of sensing-target k in the exponential domain as follows:

$$\mathcal{M}_{\mathcal{T}^{\mathrm{I}}_{u,k}(\mu-1,\mu)}(1+\theta) \leq e^{\theta\left[\rho^{\mathrm{I}}_{u,k}(\theta)+\sigma^{\mathrm{I}}_{u,k}(\theta)\right]}. \tag{40}$$

Assume that the inter-arrival times $T^{\mathrm{I}}_{u,k}(\mu-1,\mu)$, $\forall\mu$, are *independent and identically distributed* (i.i.d.) for each status-update data packet, we have

$$\mathcal{M}_{\mathcal{T}^{\mathrm{I}}_{u,k}(\mu-1,\mu)}(1+\theta) = \mathcal{M}_{\mathcal{T}^{\mathrm{I}}_{u,k}(1,2)}(1+\theta), \qquad \forall\mu. \tag{41}$$

Thus, we can obtain

$$\begin{aligned}\mathcal{M}_{\mathcal{T}^{\mathrm{I}}_{u,k}(\nu,\mu)}(1+\theta) &= \mathbb{E}\left[\prod_{j=\nu+1}^{\mu}e^{\theta T^{\mathrm{I}}_{u,k}(j-1,j)}\right]\\ &= \left(\mathbb{E}\left[e^{\theta T^{\mathrm{I}}_{u,k}(\mu-1,\mu)}\right]\right)^{(\mu-\nu)}\\ &= \left[\mathcal{M}_{\mathcal{T}^{\mathrm{I}}_{u,k}(\mu-1,\mu)}(1+\theta)\right]^{(\mu-\nu)}, \ \forall\nu\leq\mu.\end{aligned} \tag{42}$$

2) The Mellin Transform of the Service Time: Similarly, using the $(\sigma^{\mathrm{S}}(\theta),\rho^{\mathrm{S}}(\theta))$-bounded process, the Mellin transform of the cumulative service time in the exponential domain can be upper-bounded as follows:

$$\begin{aligned}\mathcal{M}_{\mathcal{T}^{\mathrm{S}}_{u,k}(\nu,\mu)}(1+\theta) &= \mathbb{E}\left[\left\{\mathcal{T}^{\mathrm{S}}_{u,k}(\nu,\mu)\right\}^{\theta}\right]\\ &\leq e^{\theta\left[(\mu-\nu+1)\rho^{\mathrm{S}}_{u,k}(\theta)+\sigma^{\mathrm{S}}_{u,k}(\theta)\right]}.\end{aligned} \tag{43}$$

Assuming that the service times $T^{\mathrm{S}}_{u,k}(\mu)$, $\forall\mu$, are i.i.d. for each status-update data packet, we can derive the Mellin transform of the service time, denoted by $\mathcal{M}_{\mathcal{T}^{\mathrm{S}}_{u,k}(\mu)}(1+\theta)$, in the exponential domain as follows:

$$\mathcal{M}_{\mathcal{T}^{\mathrm{S}}_{u,k}(\mu)}(1+\theta) = \mathcal{M}_{\mathcal{T}^{\mathrm{S}}_{u,k}(1)}(1+\theta), \qquad \forall\mu. \tag{44}$$

Thus, we can derive the Mellin transform of the cumulative service time in the exponential domain as follows:

$$\begin{aligned}\mathcal{M}_{\mathcal{T}^{\mathrm{S}}_{u,k}(\nu,\mu)}(1+\theta) &= \mathbb{E}\left[\prod_{\mu=\nu+1}^{\mu}e^{\theta T^{\mathrm{S}}_{u,k}(\mu)}\right]\\ &= \left\{\mathbb{E}\left[e^{\theta T^{\mathrm{S}}_{u,k}(\mu)}\right]\right\}^{(\mu-\nu)}\\ &= \left[\mathcal{M}_{\mathcal{T}^{\mathrm{S}}_{u,k}(\mu)}(1+\theta)\right]^{(\mu-\nu)}.\end{aligned} \tag{45}$$

Then, assuming that the inter-arrival time $T^{\mathrm{I}}_{u,k}(\mu-1,\mu)$ and service time $T^{\mathrm{S}}_{u,k}(\mu)$ are i.i.d., we can characterize the upper bound on the peak AoI violation probability, which is specified in the following theorem.

Theorem 2: **If** $\theta>0$ and the stability condition $\rho^{\mathrm{S}}_{u,k}(\theta)<\rho^{\mathrm{I}}_{u,k}(-\theta)$ hold, **then** the upper bound on the peak AoI violation probability for our proposed AoI-driven UAV schemes is given as follows:

$$\epsilon_{u,k}^{(\mu,\mathrm{AoI})} \leq \frac{e^{-\frac{\theta A_{\mathrm{th}}}{n}}\mathcal{M}_{\mathcal{T}^{\mathrm{I}}_{u,k}(\mu-1,\mu)}(1+\theta)\mathcal{M}_{\mathcal{T}^{\mathrm{S}}_{u,k}(\mu)}(1+\theta)}{1-\mathcal{M}_{\mathcal{T}^{\mathrm{I}}_{u,k}(\mu-1,\mu)}(1-\theta)\mathcal{M}_{\mathcal{T}^{\mathrm{S}}_{u,k}(\mu)}(1+\theta)}, \ \forall\mu, \tag{46}$$

when the stability condition $\mathcal{M}_{\mathcal{T}^{\mathrm{I}}_{u,k}(\mu-1,\mu)}(1-\theta)\mathcal{M}_{\mathcal{T}^{\mathrm{S}}_{u,k}(\mu)}(1+\theta)<1$ is satisfied.

Proof: Using Eqs. (37), (39), (40), and (43), we can rewrite the upper-bounded peak AoI violation probability as follows:

$$\begin{aligned}\epsilon_{u,k}^{(\mu,\mathrm{AoI})} &\leq e^{-\frac{\theta A_{\mathrm{th}}}{n}} e^{\theta\left[\rho_{u,k}^{\mathrm{I}}(\theta)+\sigma_{u,k}^{\mathrm{I}}(\theta)\right]} e^{\theta\left[\sigma_{u,k}^{\mathrm{I}}(-\theta)+\rho_{u,k}^{\mathrm{S}}(\theta)+\sigma_{u,k}^{\mathrm{S}}(\theta)\right]} \\ &\quad \times\left\{\sum_{\nu=1}^{\mu} e^{-\theta\left[\rho_{u,k}^{\mathrm{I}}(-\theta)-\rho_{u,k}^{\mathrm{S}}(\theta)\right](\mu-\nu)}\right\} \\ &\leq e^{-\frac{\theta A_{\mathrm{th}}}{n}} e^{\theta\left[\rho_{u,k}^{\mathrm{I}}(\theta)+\sigma_{u,k}^{\mathrm{I}}(\theta)\right]} e^{\theta\left[\sigma_{u,k}^{\mathrm{I}}(-\theta)+\rho_{u,k}^{\mathrm{S}}(\theta)+\sigma_{u,k}^{\mathrm{S}}(\theta)\right]} \\ &\quad \times\left\{\sum_{\nu=0}^{\infty} \left[e^{-\theta\left[\rho_{u,k}^{\mathrm{I}}(-\theta)-\rho_{u,k}^{\mathrm{S}}(\theta)\right]}\right]^{\nu}\right\} \\ &\overset{(a)}{=} \frac{e^{-\frac{\theta A_{\mathrm{th}}}{n}} e^{\theta\left[\rho_{u,k}^{\mathrm{I}}(\theta)+\sigma_{u,k}^{\mathrm{I}}(\theta)\right]} e^{\theta\left[\sigma_{u,k}^{\mathrm{I}}(-\theta)+\rho_{u,k}^{\mathrm{S}}(\theta)+\sigma_{u,k}^{\mathrm{S}}(\theta)\right]}}{1-e^{-\theta\left[\rho_{u,k}^{\mathrm{I}}(-\theta)-\rho_{u,k}^{\mathrm{S}}(\theta)\right]}}\end{aligned} \tag{47}$$

where the following stability condition must hold:

$$e^{-\theta\left[\rho_{u,k}^{\mathrm{I}}(-\theta)-\rho_{u,k}^{\mathrm{S}}(\theta)\right]}<1, \tag{48}$$

which leads to $\rho_{u,k}^{\mathrm{S}}(\theta) < \rho_{u,k}^{\mathrm{I}}(-\theta)$. Notice that (a) in Eq. (47) holds due to the infinite geometric series theorem. Furthermore, since the moment generating function (MGF) of a sum of independent random variables is the product of their MGFs, we get $\mathcal{M}_{\mathcal{X}+\mathcal{Y}}(1+\theta) = \mathcal{M}_{\mathcal{X}}(1+\theta)\mathcal{M}_{\mathcal{Y}}(1+\theta)$. Due to $\mathcal{M}_{\mathcal{T}_{u,k}^{\mathrm{I}}(\nu,\mu)}(1+\theta) = \left[\mathcal{M}_{\mathcal{T}_{u,k}^{\mathrm{I}}(\mu-1,\mu)}(1+\theta)\right]^{(\mu-\nu)}$ and $\mathcal{M}_{\mathcal{T}_{u,k}^{\mathrm{S}}(\nu,\mu)}(1+\theta) = \left[\mathcal{M}_{\mathcal{T}_{u,k}^{\mathrm{S}}(\mu)}(1+\theta)\right]^{(\mu-\nu)}$ given by Eqs. (42) and (45), respectively, the minimal traffic and service parameters can be derived from Eqs. (39) and (43) as follows [42]:

$$\begin{cases}\sigma_{u,k}^{\mathrm{I}}(\theta)=\sigma_{u,k}^{\mathrm{S}}(\theta)=0; \\ \rho_{u,k}^{\mathrm{I}}(-\theta)=-\frac{1}{\theta}\log\left\{\mathbb{E}\left[e^{-\theta T_{u,k}^{\mathrm{I}}(\mu-1,\mu)}\right]\right\}; \\ \rho_{u,k}^{\mathrm{S}}(\theta)=\frac{1}{\theta}\log\left\{\mathbb{E}\left[e^{\theta T_{u,k}^{\mathrm{S}}(\mu)}\right]\right\}.\end{cases} \tag{49}$$

By plugging the traffic and service parameters as specified in Eq. (49) back into Eq. (47), we get

$$\begin{aligned}\epsilon_{u,k}^{(\mu,\mathrm{AoI})} &\leq \frac{e^{-\frac{\theta A_{\mathrm{th}}}{n}} e^{\theta\left[\rho_{u,k}^{\mathrm{I}}(\theta)\right]} e^{\theta\left[\rho_{u,k}^{\mathrm{S}}(\theta)\right]}}{1-e^{-\theta\left[\rho_{u,k}^{\mathrm{I}}(-\theta)-\rho_{u,k}^{\mathrm{S}}(\theta)\right]}} \\ &= \frac{e^{-\frac{\theta A_{\mathrm{th}}}{n}} \mathbb{E}\left[e^{\theta T_{u,k}^{\mathrm{I}}(\mu-1,\mu)}\right]\mathbb{E}\left[e^{\theta T_{u,k}^{\mathrm{S}}(\mu)}\right]}{1-\mathbb{E}\left[e^{-\theta T_{u,k}^{\mathrm{I}}(\mu-1,\mu)}\right]\mathbb{E}\left[e^{\theta T_{u,k}^{\mathrm{S}}(\mu)}\right]} \\ &= \frac{e^{-\frac{\theta A_{\mathrm{th}}}{n}} \mathcal{M}_{\mathcal{T}_{u,k}^{\mathrm{I}}(\mu-1,\mu)}(1+\theta)\mathcal{M}_{\mathcal{T}_{u,k}^{\mathrm{S}}(\mu)}(1+\theta)}{1-\mathcal{M}_{\mathcal{T}_{u,k}^{\mathrm{I}}(\mu-1,\mu)}(1-\theta)\mathcal{M}_{\mathcal{T}_{u,k}^{\mathrm{S}}(\mu)}(1+\theta)},\end{aligned} \tag{50}$$

which yields a valid upper-bound for $\epsilon_{u,k}^{(\mu,\mathrm{AoI})}$ because the following stability condition holds:

$$\mathcal{M}_{\mathcal{T}_{u,k}^{\mathrm{I}}(\mu-1,\mu)}(1-\theta)\mathcal{M}_{\mathcal{T}_{u,k}^{\mathrm{S}}(\mu)}(1+\theta)<1. \tag{51}$$

Thus, Eq. (46) follows due to Eq. (50). Therefore, we complete the proof of Theorem 2. ■

Remarks on Theorem 2: Assuming that the inter-arrival time $T_{u,k}^{\mathrm{I}}(\mu-1,\mu)$ and service time $T_{u,k}^{\mathrm{S}}(\mu)$ are i.i.d., Theorem 2 provides with a more simplified upper-bound on the peak AoI violation probability given in Eq. (46), which will be implemented in formulating and solving the peak AoI violation probability minimization problem for our proposed AoI-driven UAV multimedia mobile networks in the finite blocklength regime as detailed in the following section.

Furthermore, since the status-update data packets are generated according to a Bernoulli process with probability $p_{u,k}(\mu)$, the inter-arrival time follows a geometric process with parameter $p_{u,k}(\mu)$. By using the MGF of a geometric process, we can derive the Mellin transform of the inter-arrival time in the exponential domain as follows:

$$\mathcal{M}_{\mathcal{T}_{u,k}^{\mathrm{I}}(\mu-1,\mu)}(1+\theta)=\frac{p_{u,k}(\mu)e^{\theta}}{1-e^{\theta}\left[1-p_{u,k}(\mu)\right]}. \tag{52}$$

Based on Eqs. (46) and (52), we have

$$\epsilon_{u,k}^{(\mu,\mathrm{AoI})} \leq \frac{p_{u,k}(\mu)e^{\theta\left(1-\frac{A_{\mathrm{th}}}{n}\right)}}{1-e^{\theta}\left[1-p_{u,k}(\mu)\right]}\mathcal{M}_{\mathcal{T}_{u,k}^{\mathrm{S}}(\mu)}(1+\theta), \quad \forall\mu. \tag{53}$$

IV. The Peak AoI Violation Probability Minimization in the Finite Blocklength Regime

In this section, taking into account the transmit power and UAV trajectory constraints, we formulate and solve the FBC based peak AoI violation probability minimization problem for our proposed AoI-driven UAV schemes.

A. The Peak AoI Violation Probability Minimization in the Finite Blocklength Regime

Denote by $\boldsymbol{B} \triangleq \{b_{u,k}(\mu), \forall\mu\in\mathsf{N}, \forall k\in\mathsf{K}, \forall u\in\mathsf{U}\}$, $\boldsymbol{\mathcal{P}} \triangleq \left\{\mathcal{P}_{u,k}^{(\mu)}, \forall\mu\in\mathsf{N}, \forall k\in\mathsf{K}, \forall u\in\mathsf{U}\right\}$, and $\boldsymbol{Q} \triangleq \{\boldsymbol{q}_{u,k}(\mu), \forall\mu\in\mathsf{N}, \forall k\in\mathsf{K}, \forall u\in\mathsf{U}\}$ the user association vector, transmit power vector, and UAV trajectory vector, respectively, for K sensing-targets at U UAVs for transmitting N status-update data packets. Based on Eq. (53), given the peak AoI threshold A_{th}, we can formulate the total peak AoI violation probability minimization problem $\mathbf{P_1}$ for transmitting N status-update data packets of K sensing-targets over our proposed AoI-driven UAV multimedia mobile networks in the finite blocklength regime as follows:

$$\begin{aligned}\mathbf{P_1}: &\arg\min_{\{\boldsymbol{B},\boldsymbol{\mathcal{P}},\boldsymbol{Q}\}}\left\{\sum_{u=1}^{U}\sum_{\mu=1}^{N}\sum_{k=1}^{K}\epsilon_{u,k}^{(\mu,\mathrm{AoI})}\right\} \\ &\leq \arg\min_{\{\boldsymbol{B},\boldsymbol{\mathcal{P}},\boldsymbol{Q}\}}\left\{\sum_{u=1}^{U}\sum_{\mu=1}^{N}\sum_{k=1}^{K} e^{-\frac{\theta A_{\mathrm{th}}}{n}}\mathcal{M}_{\mathcal{T}_{u,k}^{\mathrm{I}}(\mu-1,\mu)}(1+\theta)\right. \\ &\quad\left.\times\frac{\mathcal{M}_{\mathcal{T}_{u,k}^{\mathrm{S}}(\mu)}(1+\theta)}{1-\mathcal{M}_{\mathcal{T}_{u,k}^{\mathrm{I}}(\mu-1,\mu)}(1-\theta)\mathcal{M}_{\mathcal{T}_{u,k}^{\mathrm{S}}(\mu)}(1+\theta)}\right\}\end{aligned} \tag{54}$$

$$\text{s.t.}\quad C1: \epsilon\left(\gamma_{u,k}^{(\mu)}\right) \leq \epsilon_{\mathrm{th}}, \quad k\in\mathsf{K}; \tag{55}$$

$$C2: \sum_{k=0}^{K} b_{u,k}(\mu)\mathcal{P}_{u,k}^{(\mu)} \leq \overline{\mathcal{P}}, \quad k\in\mathsf{K}; \tag{56}$$

$$C3: \left\|\boldsymbol{q}_{u,k}(\mu+1)-\boldsymbol{q}_{u,k}(\mu)\right\| \leq V_{\max}T_{u,k}(\mu), \quad \mu=1,\ldots,(N-1), k\in\mathsf{K}; \tag{57}$$

$$C4: \left\|\boldsymbol{q}_{u,k}(\mu)-\boldsymbol{q}_{u',k}(\nu)\right\|^{2} \geq d_{\min}, \ \mu,\nu\in\mathsf{N}, k\in\mathsf{K}; \tag{58}$$

$$C5\colon \boldsymbol{q}_{u,1}(\mu) = \boldsymbol{q}_{u,\mathrm{I}}; \tag{59}$$
$$C6\colon \boldsymbol{q}_{u,(K+1)}(\mu) = \boldsymbol{q}_{u,\mathrm{F}}; \tag{60}$$
$$C7\colon p_{u,k}(\mu) \geq p_{\mathrm{th}}, \quad k \in \mathsf{K}, \tag{61}$$
$$C8\colon H_{\min} \leq z_{u,k}(\mu) \leq H_{\max}, \quad k \in \mathsf{K}; \tag{62}$$
$$C9\colon b_{u,k}(\mu) \in \{0,1\}, \quad k \in \mathsf{K}. \tag{63}$$
$$C10\colon \sum_{u=1}^{U} b_{u,k}(\mu) \leq 1, \quad k \in \mathsf{K}. \tag{64}$$

when the stability condition $\mathcal{M}_{\mathcal{T}^{\mathrm{I}}_{u,k}(\mu-1,\mu)}(1-\theta)\mathcal{M}_{\mathcal{T}^{\mathrm{S}}_{u,k}(\mu)}(1+\theta) < 1$ holds, where ϵ_{th} is the upper bound on the decoding error probability and $\overline{\mathcal{P}}$ is the average transmit power. The coupling of different optimization variables $\{\boldsymbol{B}, \boldsymbol{\mathcal{P}}, \boldsymbol{Q}\}$ makes the minimization problem $\mathbf{P_1}$ in Eq. (54) a non-convex optimization problem. In addition, $b_{u,k}(\mu)$ is a binary variable which makes $\mathbf{P_1}$ a mixed integer program. Therefore, we cannot directly solve $\mathbf{P_1}$ by using standard convex optimization techniques. We can devide the minimization problem $\mathbf{P_1}$ in Eq. (54) into the following two sub-problems and solve the minimization problem in an iterative manner.

B. Optimal Power Allocation, User Association, and UAV Trajectory Policies in the Finite Blocklength Regime

1) The Optimal Power Allocation and User Association Policy: Given the UAV trajectory $\boldsymbol{Q}$ for collecting and transmitting N status-update data packets for all K sensing-targets, we need to derive the optimal power allocation and user association policy to minimize the peak AoI violation probability. Since the inter-arrival time is known for a given UAV trajectory vector $\boldsymbol{Q}$, we can convert the optimization problem $\mathbf{P_1}$ in Eq. (54) into the following suboptimal problem:

$$\begin{aligned}\mathbf{P_2}\ &\arg\min_{\{\boldsymbol{B},\boldsymbol{\mathcal{P}}\}}\left\{\sum_{u=1}^{U}\sum_{\mu=1}^{N}\sum_{k=1}^{K}\mathcal{M}_{\mathcal{T}^{\mathrm{S}}_{u,k}(\mu)}(1+\theta)\right\}\\ &=\arg\min_{\{\boldsymbol{B},\boldsymbol{\mathcal{P}}\}}\left\{\sum_{u=1}^{U}\sum_{\mu=1}^{N}\sum_{k=1}^{K}\mathbb{E}_{\gamma^{(\mu)}_{u,k}}\left[\exp\left\{\theta T^{\mathrm{S}}_{u,k}(\mu)\right\}\right]\right\}\end{aligned} \tag{65}$$

subject to the constraints $C1$, $C2$, $C7$, $C9$, and $C10$ given in Eqs. (55), (56), (61), (63), and (64), respectively, where $\mathbb{E}_{\gamma^{(\mu)}_{u,k}}[\cdot]$ is the expectation operation over the SNR $\gamma^{(\mu)}_{u,k}$. We used the fact that the objective function in problem $\mathbf{P_1}$ in Eq. (54) is monotonically increasing in $\mathcal{M}_{\mathcal{T}^{\mathrm{S}}_{u,k}(\mu)}(1+\theta)$. Denote by T the unit time for each channel use. Since the status-update data packets may not be decoded correctly at the GBS, we apply the retransmission protocol. Using the retransmission protocol, we can derive the service time for transmitting the μth status-update data packet of sensing-target k from UAV u to the GBS as follows:

$$T^{\mathrm{S}}_{u,k}(\mu) = \frac{nT}{1-\epsilon\left(\gamma^{(\mu)}_{u,k}\right)}. \tag{66}$$

To characterize the convexity of service time $T^{\mathrm{S}}_{u,k}(\mu)$, first, we need to analyze the convexity of the decoding error probability function with respect to the SNR as detailed in the following theorem.

Theorem 3: The decoding error probability function $\epsilon(\gamma^{(\mu)}_{u,k})$ is *convex* with respect to the SNR $\gamma^{(\mu)}_{u,k}$ when $\gamma^{(\mu)}_{u,k} > 0$, $\forall\mu$.

Proof: To analyze the convexity of decoding error probability function $\epsilon(\gamma^{(\mu)}_{u,k})$, first, we define the following auxiliary function:

$$\Phi\left(\gamma^{(\mu)}_{u,k}\right) \triangleq \frac{C\left(\gamma^{(\mu)}_{u,k}\right)-\frac{\log_2 M}{n}}{\sqrt{V\left(\gamma^{(\mu)}_{u,k}\right)/n}}. \tag{67}$$

Thus, based on Eq. (17), the decoding error probability function $\epsilon(\gamma^{(\mu)}_{u,k}) \approx Q(\Phi(\gamma^{(\mu)}_{u,k}))$. Second, we obtain the first-order derivative of $\epsilon(\gamma^{(\mu)}_{u,k})$ with respect to the SNR $\gamma^{(\mu)}_{u,k}$ as follows:

$$\frac{\partial\epsilon\left(\gamma^{(\mu)}_{u,k}\right)}{\partial\gamma^{(\mu)}_{u,k}} = -\frac{1}{\sqrt{2\pi}}e^{-\frac{\Phi^2\left(\gamma^{(\mu)}_{u,k}\right)}{2}}\frac{\partial\Phi\left(\gamma^{(\mu)}_{u,k}\right)}{\partial\gamma^{(\mu)}_{u,k}}, \tag{68}$$

where

$$\begin{aligned}\frac{\partial\Phi\left(\gamma^{(\mu)}_{u,k}\right)}{\partial\gamma^{(\mu)}_{u,k}} &= \sqrt{n}\left\{\frac{1}{(\log 2)}\left[\left(\gamma^{(\mu)}_{u,k}\right)^2+2\gamma^{(\mu)}_{u,k}\right]-\log_2\left(1+\gamma^{(\mu)}_{u,k}\right)\right.\\ &\qquad\left.+\frac{\log_2 M}{n}\left\{\left[\gamma^{(\mu)}_{u,k}\left(\gamma^{(\mu)}_{u,k}+2\right)\right]^{\frac{3}{2}}\right\}^{-1}\right\}\\ &\geq \sqrt{n}\left[\frac{\left(\gamma^{(\mu)}_{u,k}+1\right)^2-1-\log\left(1+\gamma^{(\mu)}_{u,k}\right)}{(\log 2)\left[\gamma^{(\mu)}_{u,k}\left(\gamma^{(\mu)}_{u,k}+2\right)\right]^{\frac{3}{2}}}\right].\end{aligned} \tag{69}$$

Then, we define an auxiliary function, denoted by $G(x)$ ($x > 1$), as follows:

$$G(x) = x^2 - 1 - \log(x) \tag{70}$$

where $x \triangleq 1+\gamma^{(\mu)}_{u,k}$. Taking the first-order derivative of $G(x)$ with respect to x, we get

$$\frac{\partial G(x)}{\partial x} = \frac{2x^2-1}{x}. \tag{71}$$

Since $x > 1$, we can obtain $\frac{\partial G(x)}{\partial x} > 0$, i.e., function $G(x)$ is an increasing function of x when $x > 1$. Since $G(1) = 0$, we obtain $G(x) > 0$ when $x > 1$. Correspondingly, we get $\frac{\partial\Phi\left(\gamma^{(\mu)}_{u,k}\right)}{\partial\gamma^{(\mu)}_{u,k}} > 0$, which implies that the following equation holds:

$$\frac{\partial\epsilon\left(\gamma^{(\mu)}_{u,k}\right)}{\partial\gamma^{(\mu)}_{u,k}} < 0. \tag{72}$$

Thus, the decoding error probability is a monotonically decreasing function of the SNR. Third, we take the second-order derivative of function $\Phi\left(\gamma^{(\mu)}_{u,k}\right)$ with respect to $\gamma^{(\mu)}_{u,k}$ as follows:

$$\frac{\partial^2\Phi\left(\gamma^{(\mu)}_{u,k}\right)}{\partial\left[\gamma^{(\mu)}_{u,k}\right]^2} = \frac{\sqrt{n}}{\left[\gamma^{(\mu)}_{u,k}\left(\gamma^{(\mu)}_{u,k}+2\right)\right]^3}\left\{\left[\frac{1}{(\log 2)}\left(2\gamma^{(\mu)}_{u,k}+2\right)\right.\right.$$

$$-\frac{1}{(\log 2)\left(1+\gamma_{u,k}^{(\mu)}\right)}\Bigg]\left[\gamma_{u,k}^{(\mu)}\left(\gamma_{u,k}^{(\mu)}+2\right)\right]^{\frac{3}{2}}-3\Bigg\{\frac{1}{(\log 2)}\times\left[\left(\gamma_{u,k}^{(\mu)}\right)^2+2\gamma_{u,k}^{(\mu)}\right]-\log_2\left(1+\gamma_{u,k}^{(\mu)}\right)+\frac{\log_2 M}{n}\Bigg\}\times\left(1+\gamma_{u,k}^{(\mu)}\right)\left[\gamma_{u,k}^{(\mu)}\left(\gamma_{u,k}^{(\mu)}+2\right)\right]^{\frac{1}{2}}\Bigg\}$$

$$\leq\frac{\sqrt{n}}{(\log 2)\left[\gamma_{u,k}^{(\mu)}\left(\gamma_{u,k}^{(\mu)}+2\right)\right]^{\frac{3}{2}}}\Bigg\{\left(2\gamma_{u,k}^{(\mu)}+2\right)-\frac{1}{\left(1+\gamma_{u,k}^{(\mu)}\right)}-3\left[\left(\gamma_{u,k}^{(\mu)}\right)^2+2\gamma_{u,k}^{(\mu)}-\log\left(1+\gamma_{u,k}^{(\mu)}\right)\right]\frac{\left(1+\gamma_{u,k}^{(\mu)}\right)}{\gamma_{u,k}^{(\mu)}\left(\gamma_{u,k}^{(\mu)}+2\right)}\Bigg\}$$

$$=\frac{\sqrt{n}}{(\log 2)\left[\gamma_{u,k}^{(\mu)}\left(\gamma_{u,k}^{(\mu)}+2\right)\right]^{\frac{3}{2}}}\left[\frac{3\left(1+\gamma_{u,k}^{(\mu)}\right)\log\left(1+\gamma_{u,k}^{(\mu)}\right)}{\left(1+\gamma_{u,k}^{(\mu)}\right)^2-1}-\left(\gamma_{u,k}^{(\mu)}+1\right)-\frac{1}{\left(1+\gamma_{u,k}^{(\mu)}\right)}\right]. \quad (73)$$

Then, to determine whether Eq. (73) is less than zero or not, we define an auxiliary function, denoted by $F(x)$ ($x > 1$), as follows:

$$F(x)=\frac{3x\log(x)}{x^2-1}-x-\frac{1}{x} \quad (74)$$

where $x \triangleq 1+\gamma_{u,k}^{(\mu)}$. Then, taking the first-order derivative of the auxiliary function $F(x)$ with respect to x, we have

$$\frac{\partial F(x)}{\partial x}=\frac{[3\log(x)+3](x^2-1)-6x^2\log(x)}{(x^2-1)^2}-1+\frac{1}{x^2}=\frac{3x^2-3x^2\log(x)-3\log(x)-3}{(x^2-1)^2}-1+\frac{1}{x^2}. \quad (75)$$

Since $x > 1$, i.e., $\gamma_{u,k}^{(\mu)} > 0$, we can easily show that $\frac{\partial F(x)}{\partial x} < 0$, which implies that the function $F(x)$ is a monotonically decreasing function of x when $x > 1$. Since $\lim_{x\to 1^+} F(x) = -\frac{1}{2} < 0$ and $F(x)$ is a monotonically decreasing function of x when $x > 1$, using the fact that $F(x)$ is a continuous function over x for $x > 1$, we can obtain $F(x) < 0$ when $x > 1$, implying that the following equation holds:

$$\frac{\partial^2\Phi\left(\gamma_{u,k}^{(\mu)}\right)}{\partial\left[\gamma_{u,k}^{(\mu)}\right]^2}<0 \quad (76)$$

when $\gamma_{u,k}^{(\mu)} > 0$. Finally, using Eqs. (68), (69), and (73), we can obtain the second-order derivative of $\epsilon(\gamma_{u,k}^{(\mu)})$ with respect to $\gamma_{u,k}^{(\mu)}$ as follows:

$$\frac{\partial^2\epsilon\left(\gamma_{u,k}^{(\mu)}\right)}{\partial\left[\gamma_{u,k}^{(\mu)}\right]^2}=\frac{1}{\sqrt{2\pi}}e^{-\frac{\Phi^2\left(\gamma_{u,k}^{(\mu)}\right)}{2}}\left\{\Phi\left(\gamma_{u,k}^{(\mu)}\right)\left[\frac{\partial\Phi\left(\gamma_{u,k}^{(\mu)}\right)}{\partial\gamma_{u,k}^{(\mu)}}\right]^2-\frac{\partial^2\Phi\left(\gamma_{u,k}^{(\mu)}\right)}{\partial\left[\gamma_{u,k}^{(\mu)}\right]^2}\right\}>0, \quad (77)$$

which implies that the decoding error probability $\epsilon(\gamma_{u,k}^{(\mu)})$ is a convex function with respect to the SNR $\gamma_{u,k}^{(\mu)}$ when $\gamma_{u,k}^{(\mu)} > 0$. Therefore, we complete the proof of Theorem 3. ■

Remarks on Theorem 3: Since the SNR is a linear function of the transmit power $\mathcal{P}_{u,k}^{(\mu)}$, Theorem 3 implies that the decoding error probability function $\epsilon\left(\gamma_{u,k}^{(\mu)}\right)$ is convex in the transmit power $\mathcal{P}_{u,k}^{(\mu)}$. Then, we need to analyze the convexity of the service time $T_{u,k}^{\mathrm{S}}(\mu)$ with respect to the SNR, motivating the following theorem.

Theorem 4: **If** the decoding error probability function $\epsilon(\gamma_{u,k}^{(\mu)})$ and service time $T_{u,k}^{\mathrm{S}}(\mu)$ are characterized by Eq. (17) and (66), respectively, **then** the following claims hold for our proposed AoI-driven UAV schemes in the finite blocklength regime.

Claim 1. The service time $T_{u,k}^{\mathrm{S}}(\mu)$ is *convex* with respect to the decoding error probability function $\epsilon\left(\gamma_{u,k}^{(\mu)}\right)$, $\forall\mu$.

Claim 2. The service time $T_{u,k}^{\mathrm{S}}(\mu)$ is *convex* with respect to the SNR $\gamma_{u,k}^{(\mu)}$ when $\gamma_{u,k}^{(\mu)} > 0$, $\forall\mu$.

Proof: We proceed with the proof by showing Claim 1 and Claim 2, respectively.

Claim 1. To analyze the convexity of the service time $T_{u,k}^{\mathrm{S}}(\mu)$ in the decoding error probability function $\epsilon\left(\gamma_{u,k}^{(\mu)}\right)$, first, we obtain the first-order derivative of $T_{u,k}^{\mathrm{S}}(\mu)$ with respect to the SNR $\gamma_{u,k}^{(\mu)}$ as follows:

$$\frac{\partial T_{u,k}^{\mathrm{S}}(\mu)}{\partial\gamma_{u,k}^{(\mu)}}=\frac{\partial T_{u,k}^{\mathrm{S}}(\mu)}{\partial\epsilon\left(\gamma_{u,k}^{(\mu)}\right)}\frac{\partial\epsilon\left(\gamma_{u,k}^{(\mu)}\right)}{\partial\gamma_{u,k}^{(\mu)}} \quad (78)$$

where

$$\frac{\partial T_{u,k}^{\mathrm{S}}(\mu)}{\partial\epsilon\left(\gamma_{u,k}^{(\mu)}\right)}=\frac{nT}{\left[1-\epsilon\left(\gamma_{u,k}^{(\mu)}\right)\right]^2}>0 \quad (79)$$

which implies that $T_{u,k}^{\mathrm{S}}(\mu)$ is an increasing function with respect to $\epsilon\left(\gamma_{u,k}^{(\mu)}\right)$. Second, we obtain the second-order derivative of $T_{u,k}^{\mathrm{S}}(\mu)$ with respect to the decoding error probability function $\epsilon\left(\gamma_{u,k}^{(\mu)}\right)$ as follows:

$$\frac{\partial^2 T_{u,k}^{\mathrm{S}}(\mu)}{\partial\left[\epsilon\left(\gamma_{u,k}^{(\mu)}\right)\right]^2}=\frac{2nT}{\left[1-\epsilon\left(\gamma_{u,k}^{(\mu)}\right)\right]^3}>0, \quad (80)$$

implying that the service time $T_{u,k}^{\mathrm{S}}(\mu)$ is a convex function with respect to the decoding error probability function $\epsilon(\gamma_{u,k}^{(\mu)})$, $\forall\mu$. Thus, we complete the proof of Claim 1 in Theorem 4.

Claim 2. Using chain rule, we obtain the second-order derivative of $T_{u,k}^{\mathrm{S}}(\mu)$ with respect to the SNR $\gamma_{u,k}^{(\mu)}$ as follows:

$$\frac{\partial^2 T_{u,k}^{\mathrm{S}}(\mu)}{\partial\left[\gamma_{u,k}^{(\mu)}\right]^2}=\frac{\partial^2 T_{u,k}^{\mathrm{S}}(\mu)}{\partial\left[\epsilon\left(\gamma_{u,k}^{(\mu)}\right)\right]^2}\left[\frac{\partial\epsilon\left(\gamma_{u,k}^{(\mu)}\right)}{\partial\gamma_{u,k}^{(\mu)}}\right]^2+\frac{\partial T_{u,k}^{\mathrm{S}}(\mu)}{\partial\epsilon\left(\gamma_{u,k}^{(\mu)}\right)}\frac{\partial^2\epsilon\left(\gamma_{u,k}^{(\mu)}\right)}{\partial\left[\gamma_{u,k}^{(\mu)}\right]^2}>0. \quad (81)$$

Equation (81) implies that the service time $T_{u,k}^{\mathrm{S}}(\mu)$ is a convex function with respect to the SNR $\gamma_{u,k}^{(\mu)}$ when

$\gamma_{u,k}^{(\mu)} > 0, \forall \mu$. Therefore, we complete the proof of Claim 2 in Theorem 4. ■

Remarks on Theorem 4: Since the SNR is a linear function of $\mathcal{P}_{u,k}^{(\mu)}$, Theorem 4 implies that the service time $T_{u,k}^{\mathrm{S}}(\mu)$ is convex in $\mathcal{P}_{u,k}^{(\mu)}$.

Using the results given in Theorem 4, we can apply the Jensen's inequality and obtain the following equations:

$$\begin{aligned}\mathcal{M}_{\mathcal{T}_{u,k}^{\mathrm{S}}(\mu)}(1+\theta) =&\ \mathbb{E}_{\gamma_{u,k}^{(\mu)}}\left[\exp\left\{\theta T_{u,k}^{\mathrm{S}}(\mu)\right\}\right] \\ \geq&\ \exp\left\{\theta \mathbb{E}_{\gamma_{u,k}^{(\mu)}}\left[T_{u,k}^{\mathrm{S}}(\mu)\right]\right\}. \end{aligned} \tag{82}$$

Since the SNR is a linear function of $\mathcal{P}_{u,k}^{(\mu)}$, Theorem 4 implies that the objective function of the minimization problem $\mathbf{P_2}$ given by Eq. (65) is convex in $\mathcal{P}_{u,k}^{(\mu)}$. However, the constraint $C1$ specified by Eq. (55) is still non-convex. Towards this end, we define the following auxiliary function:

$$\Psi\left(\gamma_{u,k}^{(\mu)}\right) \triangleq \epsilon\left(\gamma_{u,k}^{(\mu)}\right). \tag{83}$$

Based on Eq. (72), the decoding error probability function $\epsilon\left(\gamma_{u,k}^{(\mu)}\right)$ is decreasing with respect to the SNR, which equivalently implies that the auxiliary function $\Psi\left(\gamma_{u,k}^{(\mu)}\right)$ is decreasing with respect to the SNR $\gamma_{u,k}^{(\mu)}$. We can then convert the inequality in constraint $C1$ given by Eq. (55) into an equivalent constraint $C1'$ as follows:

$$C1' : \gamma_{u,k}^{(\mu)} \geq \Psi^{-1}\left(\epsilon_{\mathrm{th}}\right) \tag{84}$$

where $\Psi^{-1}(\cdot)$ is the inverse of the function $\Psi\left(\gamma_{u,k}^{(\mu)}\right)$ given in Eq. (83). Using Eqs. (8) and (84), we have

$$C1'' : \mathcal{P}_{u,k}^{(\mu)} \leq \frac{\sigma^2\left(\left\|\widetilde{\boldsymbol{q}}_{u,k}(\mu)\right\|^2 + \left[z_{u,k}(\mu)\right]^2\right)\Psi^{-1}\left(\epsilon_{\mathrm{th}}\right)}{\beta_0}, \tag{85}$$

which is convex with respect to the transmit power $\mathcal{P}_{u,k}^{(\mu)}$. As a result, the minimization problem $\mathbf{P_2}$ given by Eq. (65) subject to the constraints $C1''$, $C2$, $C9$, and $C10$ given in Eqs. (55), (56), (63), and (64), respectively, is a mixed integer disciplined convex program (MIDCP) problem which obeys the same convexity rules as standard disciplined convex programs (DCPs). This implies that there exists a unique optimal solution that minimizes problem $\mathbf{P_2}$ and the global optimum can be efficiently found by the combination of a traditional convex optimization algorithm with an exhaustive search, such as branch and bound algorithm which can quickly and efficiently find the optimal solution when the limits are set appropriately. This can be done by applying the CVX toolbox [43].

2) The Optimal UAV Trajectory Policy: Once the optimal power and user association allocation policy is selected in the previous step, the minimization problem $\mathbf{P_1}$ specified by Eq. (54) becomes a feasible optimization problem in $\boldsymbol{Q}$. Therefore, we need to find the optimal UAV trajectory policy to minimize the peak AoI violation probability. We can convert the minimization problem $\mathbf{P_1}$ into a suboptimal problem $\mathbf{P_3}$ as follows:

$$\begin{aligned}\mathbf{P_3}: \arg\min_{\boldsymbol{Q}} \Bigg\{ &\sum_{u=1}^{U}\sum_{\mu=1}^{N}\sum_{k=1}^{K} e^{-\frac{\theta A_{\mathrm{th}}}{n}} \mathcal{M}_{\mathcal{T}_{u,k}^{\mathrm{I}}(\mu-1,\mu)}(1+\theta) \\ &\times \frac{\mathcal{M}_{\mathcal{T}_{u,k}^{\mathrm{S}}(\mu)}(1+\theta)}{1-\mathcal{M}_{\mathcal{T}_{u,k}^{\mathrm{I}}(\mu-1,\mu)}(1-\theta)\mathcal{M}_{\mathcal{T}_{u,k}^{\mathrm{S}}(\mu)}(1+\theta)}\Bigg\}\end{aligned} \tag{86}$$

subject to the constraints $C1''$ and $C3 - C10$ given in Eqs. (85) and (57)-(64), respectively. To solve the minimization problem $\mathbf{P_3}$ in Eq. (86), first, we need to characterize the convexity of the Mellin transforms of the inter-arrival time $\mathcal{M}_{\mathcal{T}_{u,k}^{\mathrm{I}}(\mu-1,\mu)}(1+\theta)$ and $\mathcal{M}_{\mathcal{T}_{u,k}^{\mathrm{I}}(\mu-1,\mu)}(1-\theta)$ in the exponential domain with respect to distance $d_{u,k}(\mu)$, respectively, which motivates the following theorem.

Theorem 5: The Mellin transform of the inter-arrival time $\mathcal{M}_{\mathcal{T}_{u,k}^{\mathrm{I}}(\mu-1,\mu)}(1+\theta)$ in the exponential domain is *convex* with respect to distance $d_{u,k}(\mu)$, $\forall\mu$.

Proof: Using Eqs. (19) and (52), we can obtain the first-order derivative of $\mathcal{M}_{\mathcal{T}_{u,k}^{\mathrm{I}}(\mu-1,\mu)}(1+\theta)$ with respect to the distance $d_{u,k}(\mu)$ between the UAV and mobile device k as follows:

$$\frac{\partial \mathcal{M}_{\mathcal{T}_{u,k}^{\mathrm{I}}(\mu-1,\mu)}(1+\theta)}{\partial d_{u,k}(\mu)} = \frac{\partial \mathcal{M}_{\mathcal{T}_{u,k}^{\mathrm{I}}(\mu-1,\mu)}(1+\theta)}{\partial p_{u,k}(\mu)}\frac{\partial p_{u,k}(\mu)}{\partial d_{u,k}(\mu)} \tag{87}$$

where

$$\frac{\partial \mathcal{M}_{\mathcal{T}_{u,k}^{\mathrm{I}}(\mu-1,\mu)}(1+\theta)}{\partial p_{u,k}(\mu)} = \frac{e^{\theta}\left(1-e^{\theta}\right)}{\left\{1-e^{\theta}\left[1-p_{u,k}(\mu)\right]\right\}^2}, \tag{88}$$

and

$$\frac{\partial p_{u,k}(\mu)}{\partial d_{u,k}(\mu)} = -\xi e^{-\xi d_{u,k}(\mu)} < 0. \tag{89}$$

Since $1 - e^{\theta} < 0$, we can obtain $\frac{\partial \mathcal{M}_{\mathcal{T}_{u,k}^{\mathrm{I}}(\mu-1,\mu)}(1+\theta)}{\partial d_{u,k}(\mu)} > 0$. Using chain rule, we obtain the second-order derivative of $\mathcal{M}_{\mathcal{T}_{u,k}^{\mathrm{I}}(\mu-1,\mu)}(1+\theta)$ with respect to $d_{u,k}(\mu)$ as follows:

$$\begin{aligned}&\frac{\partial^2 \mathcal{M}_{\mathcal{T}_{u,k}^{\mathrm{I}}(\mu-1,\mu)}(1+\theta)}{\partial\left[d_{u,k}(\mu)\right]^2} \\ &\quad= \frac{\partial^2 \mathcal{M}_{\mathcal{T}_{u,k}^{\mathrm{I}}(\mu-1,\mu)}(1+\theta)}{\partial\left[p_{u,k}(\mu)\right]^2}\left[\frac{\partial p_{u,k}(\mu)}{\partial d_{u,k}(\mu)}\right]^2 \\ &\qquad+ \frac{\partial \mathcal{M}_{\mathcal{T}_{u,k}^{\mathrm{I}}(\mu-1,\mu)}(1+\theta)}{\partial p_{u,k}(\mu)}\frac{\partial^2 p_{u,k}(\mu)}{\partial\left[d_{u,k}(\mu)\right]^2}\end{aligned} \tag{90}$$

where

$$\frac{\partial^2 \mathcal{M}_{\mathcal{T}_{u,k}^{\mathrm{I}}(\mu-1,\mu)}(1+\theta)}{\partial\left[p_{u,k}(\mu)\right]^2} = \frac{-2e^{2\theta}\left(1-e^{\theta}\right)}{\left\{1-e^{\theta}\left[1-p_{u,k}(\mu)\right]\right\}^3}, \tag{91}$$

and

$$\frac{\partial^2 p_{u,k}(\mu)}{\partial\left[d_{u,k}(\mu)\right]^2} = (\xi)^2 e^{-\xi d_{u,k}(\mu)} > 0. \tag{92}$$

Since $1 - e^{\theta}\left[1-p_{u,k}(\mu)\right] > 0$, we can show that $\frac{\partial^2 \mathcal{M}_{\mathcal{T}_{u,k}^{\mathrm{I}}(\mu-1,\mu)}(1+\theta)}{\partial\left[p_{u,k}(\mu)\right]^2} > 0$. Therefore, we also obtain that

$\frac{\partial^2 \mathcal{M}_{\mathcal{T}^{\mathrm{I}}_{u,k}(\mu-1,\mu)}(1+\theta)}{\partial[d_{u,k}(\mu)]^2} > 0$, implying that the Mellin transform of the inter-arrival time $\mathcal{M}_{\mathcal{T}^{\mathrm{I}}_{u,k}(\mu-1,\mu)}(1+\theta)$ in the exponential domain is convex with respect to the transmission distance $d_{u,k}(\mu)$. Therefore, we complete the proof of Theorem 5. ■

Remarks on Theorem 5: Due to $d_{u,k}(\mu) = \left\|\boldsymbol{q}_{u,k}(\mu) - \boldsymbol{q}_{\mathrm{G},k}\right\|$, Theorem 5 implies that the Mellin transform of the inter-arrival time $\mathcal{M}_{\mathcal{T}^{\mathrm{I}}_{u,k}(\mu-1,\mu)}(1+\theta)$ is convex with respect to $\boldsymbol{q}_{u,k}(\mu)$. Similarly, we can obtain that the Mellin transform of the inter-arrival time $\mathcal{M}_{\mathcal{T}^{\mathrm{I}}_{u,k}(\mu-1,\mu)}(1-\theta)$ is convex with respect to $\boldsymbol{q}_{u,k}(\mu)$. Second, we need to analyze the convexity of the Mellin transform of the service time $\mathcal{M}_{\mathcal{T}^{\mathrm{S}}_{u,k}(\mu)}(1+\theta)$ in the exponential domain with respect to $\boldsymbol{q}_{u,k}(\mu)$. Based on Eq. (82), it is equivalent to analyze the convexity of $T^{\mathrm{S}}_{u,k}(\mu)$ with respect to $\boldsymbol{q}_{u,k}(\mu)$. Claim 2 of Theorem 4 has shown that the service time $T^{\mathrm{S}}_{u,k}(\mu)$ is convex with respect to the SNR $\gamma^{(\mu)}_{u,k}$ when $\gamma^{(\mu)}_{u,k} > 0$. Using Eq. (8), we obtain that the SNR $\gamma^{(\mu)}_{u,k}$ is convex with respect to $\boldsymbol{q}_{u,k}(\mu)$ when $\gamma^{(\mu)}_{u,k} > 0$, which implies that the service time $T^{\mathrm{S}}_{u,k}(\mu)$ is convex in $\boldsymbol{q}_{u,k}(\mu)$, $\forall\mu$. Third, we can easily show that the constraints $C1''$ and $C7$ are both convex in $\boldsymbol{q}_{u,k}(\mu)$. Therefore, we can show that the objective function of the minimization problem $\mathbf{P_3}$ given by Eq. (86) is convex with respect to $\boldsymbol{q}_{u,k}(\mu)$ under the constraints $C1''$ and $C3 - C10$ given in Eqs. (85) and (57)-(64), respectively. As a result, the minimization problem $\mathbf{P_3}$ in Eq. (86) can be solved by using the conventional exhaustive search algorithms can find the optimal solutions for each sub-problem in an iterative manner. However, the time efficiency of the exhaustive search method may be poor and the computational complexity will increase dramatically as the problem size becomes larger, which may impose some application limitation for mURLLC traffics. Therefore, we develop the Recursive Uniform Search (RUS) algorithm, which is a modified version of Recursive Random Search (RRS) algorithm [44]. There are several advantages for the RUS algorithm, such as faster convergence, lower computational complexity, and fewer parameters, as compared with exhaustive search algorithms. Thus, we develop an RUS based algorithm as shown in **Algorithm 1** to solve the minimization problem $\mathbf{P_1}$ given by Eq. (54) for our proposed AoI-driven UAV schemes in the finite blocklength regime.

Our algorithm starts by generating a set of initial I high-efficiency future/next position candidates, denoted by $\boldsymbol{q}^{(i)}_{u,k}(\mu+1)$, for $i = 1, \ldots, I$, to identify promising candidates and form initial population set, denoted by I, with the set cardinality: $|\mathsf{I}| = I$ for set I. These candidates need to satisfy the trajectory constraints $C3 - C6$ given in Eqs. (57)-(60), respectively. Then, we determine the objective function achieved by each candidate position by solving the MIDCP optimization problem. We find the initial optimal local candidate, denoted by $i^{(\ell,\mathrm{local})}(\mu)$, which provides the highest solution in the ℓth iteration ($\ell = 0, 1, \ldots, L_{\max}$), where $L_{\max}$ is the predetermined maximum number of iterations. Furthermore, we start recursive sampling with uniform distribution in these areas. Using shrink-and-realign sample spaces process to find the optimal solution, denoted by $i^{\mathrm{opt}}(\mu)$, and the corresponding optimal trajectory, denoted by $\boldsymbol{q}^{(i^{\mathrm{opt}})}_{u,k}(\mu+1)$. Then, the proposed shrink-and-realign procedure is repeated until the size of the sample space decreases below a threshold, denoted by τ.

Algorithm 1 : Recursive Random Search (RRS) Based Algorithm for Solving $\mathbf{P_1}$ in Eq. (54)

Input: $K, N, U, A_{\mathrm{th}}, \epsilon_{th}, n, M, T, \xi, \overline{\mathcal{P}}, V_{\max}, H_{\min}, H_{\max}$, $\boldsymbol{q}_{u,\mathrm{I}}, \boldsymbol{q}_{u,\mathrm{F}}$, iteration tolerance threshold τ;
Initialization: $\left\{\boldsymbol{B}^{(0)}, \boldsymbol{\mathcal{P}}^{(0)}, \boldsymbol{Q}^{(0)}\right\}$
for $\mu = 1, \ldots, N$ **do**
  Set $\ell = 1$
  Generate an initial population set I, which consists of I candidates $\boldsymbol{q}^{(i)}_{u,k}(\mu+1)$, $i = 1, \ldots, I$, that satisfies the trajectory constraints $C3 - C6$ given in Eqs. (57)-(60), respectively;
  Repeat
  for $i = 1, \ldots, I$ **do**
    Given $\boldsymbol{Q}^{(\ell)}$, calculate $\boldsymbol{\mathcal{P}}^{(\ell+1)}$ and $\boldsymbol{B}^{(\ell+1)}$ by solving the MIDCP optimization problem $\mathbf{P_2}$ in Eq. (65) using CVX toolbox;
    Compute the corresponding objective function;
  end for
  Find the best local candidate $i^{\mathrm{opt}}(\mu)$ that results in the highest objective function in the ℓth iteration;
  Start recursive sampling with uniform distribution in these areas and use shrink-and-realign sample spaces process to find the best solution;
  $\ell \leftarrow (\ell+1)$;
end for
Until The fractional increase of the objective function in Eq. (54) is no larger than the iteration tolerance threshold τ.

V. Joint Optimization and Tradeoff Modeling for Peak AoI Violation Probability and ϵ-Effective Capacity Over AoI-Driven UAV Mobile Networks Using FBC

In this section, we apply the Mellin transform of the service process in the exponential domain to jointly optimize the peak AoI violation probability and ϵ-effective capacity and characterize their tradeoff in supporting our proposed statistical delay and error-rate bounded QoS provisioning over AoI-driven UAV multimedia mobile networks in the finite blocklength regime.

A. Joint Peak AoI Violation Probability and ϵ-Effective Capacity Optimization Using FBC

Statistical delay-bounded QoS guarantees [45] have been extensively studied for analyzing queuing behavior for time-varying arrival and service processes. Traditionally, the effective capacity measures queuing process which is independent of the decoding error at the receiver.

Definition 3: Based on the Large Deviation Principle (LDP), under sufficient conditions, the queueing process Q converges in distribution to a random variable $Q(\infty)$ such that

$$-\lim_{Q_{\text{th}}\to\infty}\frac{\log\left(\Pr\left\{Q(\infty)>Q_{\text{th}}\right\}\right)}{Q_{\text{th}}}=\theta \tag{93}$$

where Q_{th} represents the overflow threshold and $\theta > 0$ is defined as the *QoS exponent*, which measures the exponential decay rate of the delay-bounded QoS violation probabilities.

To be more specific, Eq. (93) states that the probability of the queuing process exceeding a certain threshold Q_{th} decays exponentially fast as the threshold Q_{th} increases. A smaller θ corresponds to a slower decay rate, which implies that the system can only provide a looser QoS guarantee, while a larger θ leads to a faster decay rate, which means that a more stringent QoS can be supported. In particular, when $\theta\to 0$, the system can tolerate an arbitrarily long delay; when $\theta\to\infty$, the system cannot tolerate any delay.

Definition 4: The *effective capacity*, denoted by $EC_{u,k}^{(\mu)}(\theta)$, for transmitting the μth status-update data packet of sensing-target k from UAV u to the GBS is defined as the maximum constant arrival rate for a given service process subject to statistical delay-bounded QoS constraints, which is given as follows:

$$EC_{u,k}^{(\mu)}(\theta)=-\tfrac{1}{\theta}\log\left\{\mathbb{E}_{\gamma_{u,k}^{(\mu)}}\left[e^{-\theta R\left(\gamma_{u,k}^{(\mu)}\right)}\right]\right\} \tag{94}$$

where $R\left(\gamma_{u,k}^{(\mu)}\right)$ is given by Eq. (16). However, the effective capacity only considers statistical delay-bounded QoS constraints. For our proposed AoI-driven UAV schemes, we introduce the new concept of ϵ*-effective capacity* for statistical delay and error-rate bounded QoS provisioning in supporting 6G mURLLC in the finite blocklength regime. To characterize the ϵ-effective capacity function, we need to first derive the service process, denoted by $S_{u,k}(\mu)$, for transmitting the μth status-update data packet of sensing-target k from UAV u to the GBS in the bit domain as follows:

$$S_{u,k}(\mu)=\begin{cases}\log_2 M, & \text{with probability } 1-\epsilon\left(\gamma_{u,k}^{(\mu)}\right);\\ 0, & \text{with probability } \epsilon\left(\gamma_{u,k}^{(\mu)}\right),\end{cases} \tag{95}$$

where $\epsilon\left(\gamma_{u,k}^{(\mu)}\right)$ is given by Eq. (17). Then, we derive the Mellin transform of the service process, denoted by $\mathcal{M}_{\mathcal{S}_{u,k}(\mu)}(\theta)$, from UAV u to the GBS in the exponential domain as follows:

$$\begin{aligned}&\mathcal{M}_{\mathcal{S}_{u,k}(\mu)}(\theta)\\&\quad=\mathbb{E}_{\gamma_{u,k}^{(\mu)}}\left[e^{(\theta-1)S_{u,k}(\mu)}\right]\\&\quad=\mathbb{E}_{\gamma_{u,k}^{(\mu)}}\left[\epsilon\left(\gamma_{u,k}^{(\mu)}\right)\right]+\mathbb{E}_{\gamma_{u,k}^{(\mu)}}\left[1-\epsilon\left(\gamma_{u,k}^{(\mu)}\right)\right]e^{(\theta-1)\log_2 M}.\end{aligned} \tag{96}$$

Thus, using Eq. (96), we obtain the definition expression for the ϵ-effective capacity with the (n,M,ϵ)-code as follows.

Definition 5: For an (n,M,ϵ)-code, the ϵ*-effective capacity*, denoted by $EC_{u,k}^{(\epsilon,\mu)}(\theta)$, for transmitting the μth status-update data packet of sensing-target k from UAV u to the GBS is defined as the maximum constant arrival rate for a given service process considering the non-vanishing decoding error-probability $\epsilon\left(\gamma_{u,k}^{(\mu)}\right)$ subject to statistical delay and error-rate bounded QoS constraints, which is given as follows:

$$\begin{aligned}&EC_{u,k}^{(\epsilon,\mu)}(\theta)\\&\triangleq-\frac{1}{n\theta}\log\left\{\mathcal{M}_{\mathcal{S}_{u,k}(\mu)}(1-\theta)\right\}\\&=-\frac{1}{n\theta}\log\Big\{\mathbb{E}_{\gamma_{u,k}^{(\mu)}}\left[\epsilon\left(\gamma_{u,k}^{(\mu)}\right)\right]+\mathbb{E}_{\gamma_{u,k}^{(\mu)}}\left[1-\epsilon\left(\gamma_{u,k}^{(\mu)}\right)\right]e^{-\theta\log_2 M}\Big\}\end{aligned} \tag{97}$$

where $\epsilon\left(\gamma_{u,k}^{(\mu)}\right)$ is given by Eq. (17).

Since our goal is to simultaneously optimize both the peak AoI violation probability and the ϵ-effective capacity over a feasible set determined by constraint functions, how to balance these two optimization problems falls into the category of an *multi-objective optimization problem* (MOP) [46]. Based on the definition for the ϵ-effective capacity, we can formulate a *joint optimization* problem $\mathbf{P_4}$ of the peak AoI violation probability and the ϵ-effective capacity for statistical delay and error-rate bounded QoS provisioning over our proposed AoI-driven UAV multimedia mobile networks in the finite blocklength regime as in the following equation:

$$\begin{aligned}\mathbf{P_4}:\ &\arg\min_{\{\boldsymbol{B},\boldsymbol{\mathcal{P}},\boldsymbol{Q}\}}\left\{\sum_{u=1}^{U}\sum_{\mu=1}^{N}\sum_{k=1}^{K}\epsilon_{u,k}^{(\mu,\text{AoI})}\right\}\\&\text{and }\arg\max_{\{\boldsymbol{B},\boldsymbol{\mathcal{P}},\boldsymbol{Q}\}}\left\{\sum_{u=1}^{U}\sum_{\mu=1}^{N}\sum_{k=1}^{K}EC_{u,k}^{(\epsilon,\mu)}(\theta)\right\}\end{aligned} \tag{98}$$

subject to the constraints $C1''$ and $C2-C10$ given in Eqs. (85) and (56)-(64), respectively. Similar to the peak AoI minimization problem as discussed in Section IV, we can iteratively solve the minimization problem $\mathbf{P_4}$ by converting it into two sub-problems as follows.

B. Optimal Power Allocation, User Association, and UAV Trajectory Policies in the Finite Blocklength Regime

1) The Optimal Power Allocation and Optimal User Association Policy: Given the UAV trajectory $\boldsymbol{Q}$, we need to find the optimal power allocation and user association policy to solve the joint optimization problem $\mathbf{P_4}$ given by Eq. (98). Similar to the suboptimal problem $\mathbf{P_2}$ given by Eq. (65) in Section IV, we can convert the optimization problem $\mathbf{P_4}$ into the following MOP $\mathbf{P_5}$:

$$\begin{aligned}\mathbf{P_5}:\ &\arg\min_{\{\boldsymbol{B},\boldsymbol{\mathcal{P}}\}}\left\{\sum_{u=1}^{U}\sum_{\mu=1}^{N}\sum_{k=1}^{K}\mathcal{M}_{\mathcal{T}_{u,k}^{\text{s}}(\mu)}(1+\theta)\right\}\\&\text{and }\arg\max_{\{\boldsymbol{B},\boldsymbol{\mathcal{P}}\}}\left\{\sum_{u=1}^{U}\sum_{\mu=1}^{N}\sum_{k=1}^{K}EC_{u,k}^{(\epsilon,\mu)}(\theta)\right\}\end{aligned} \tag{99}$$

subject to the constraints $C1''$, $C2$, $C7$, $C9$, and $C10$ given in Eqs. (85), (56), (61), (63), and (64), respectively. Based on Eq. (97), we can convert the ϵ-effective capacity maximization in MOP $\mathbf{P_5}$ into the following equivalent joint minimization problem:

$$\mathbf{P_6}: \arg\min_{\{\boldsymbol{B},\boldsymbol{\mathcal{P}}\}} \left\{\sum_{u=1}^{U}\sum_{\mu=1}^{N}\sum_{k=1}^{K}\mathcal{M}_{\mathcal{T}^{\mathrm{s}}_{u,k}(\mu)}(1+\theta)\right\}$$
$$\text{and } \arg\min_{\{\boldsymbol{B},\boldsymbol{\mathcal{P}}\}} \left\{\sum_{u=1}^{U}\sum_{\mu=1}^{N}\sum_{k=1}^{K}\mathcal{M}_{\mathcal{S}_{u,k}(\mu)}(1-\theta)\right\} \quad (100)$$

subject to the constraints $C1''$, $C2$, $C7$, $C9$, and $C10$ given in Eqs. (85), (56), (61), (63), and (64), respectively. To solve the joint minimization problem $\mathbf{P_6}$, we need to proceed with the following three steps.

First, we derive the first-order derivative of $\mathcal{M}_{\mathcal{S}_{u,k}(\mu)}(1-\theta)$ with respect to the SNR $\gamma_{u,k}^{(\mu)}$ as follows:

$$\frac{\partial \mathcal{M}_{\mathcal{S}_{u,k}(\mu)}(1-\theta)}{\partial \gamma_{u,k}^{(\mu)}} = \frac{\partial \mathcal{M}_{\mathcal{S}_{u,k}(\mu)}(1-\theta)}{\partial \epsilon\left(\gamma_{u,k}^{(\mu)}\right)}\frac{\partial \epsilon\left(\gamma_{u,k}^{(\mu)}\right)}{\partial \gamma_{u,k}^{(\mu)}}$$
$$= \left(1-e^{-\theta\log_2 M}\right)\frac{\partial \epsilon\left(\gamma_{u,k}^{(\mu)}\right)}{\partial \gamma_{u,k}^{(\mu)}}. \quad (101)$$

Since $1-e^{-\theta\log_2 M} > 0$ for $\theta > 0$ and $\frac{\partial \epsilon\left(\gamma_{u,k}^{(\mu)}\right)}{\partial \gamma_{u,k}^{(\mu)}} < 0$ specified by Eq. (72), we obtain $\frac{\partial \mathcal{M}_{\mathcal{S}_{u,k}(\mu)}(1-\theta)}{\partial \gamma_{u,k}^{(\mu)}} < 0$, which implies that $\mathcal{M}_{\mathcal{S}_{u,k}(\mu)}(1-\theta)$ is a decreasing function of the SNR $\gamma_{u,k}^{(\mu)}$. On the other hand, since we have shown that $\mathcal{M}_{\mathcal{T}^{\mathrm{s}}_{u,k}(\mu)}(1+\theta)$ is an increasing function with respect to $\epsilon\left(\gamma_{u,k}^{(\mu)}\right)$ in Section IV, we can observe that there is a *tradeoff* between $\mathcal{M}_{\mathcal{T}^{\mathrm{s}}_{u,k}(\mu)}(1+\theta)$, dictating the peak AoI violation probability, and $\mathcal{M}_{\mathcal{S}_{u,k}(\mu)}(1-\theta)$, dictating the ϵ-effective capacity, where $\mathcal{M}_{\mathcal{T}^{\mathrm{s}}_{u,k}(\mu)}(1+\theta)$ intends to monotonically decrease and $EC_{u,k}^{(\epsilon,\mu)}(\theta)$ intends to monotonically increase as the decoding error probability function $\epsilon\left(\gamma_{u,k}^{(\mu)}\right) \to 0$.

Second, in order to solve the MOP $\mathbf{P_6}$ and to achieve the Pareto optimal solutions, we apply the weighted sum method [47] to convert the MOP into a single-objective optimization problem (SOP). As a result, the joint optimization problem $\mathbf{P_6}$ given by Eq. (100) can be transformed into the following optimization problem:

$$\mathbf{P_7}: \arg\min_{\{\boldsymbol{B},\boldsymbol{\mathcal{P}}\}} \left\{\sum_{u=1}^{U}\sum_{\mu=1}^{N}\sum_{k=1}^{K}\lambda\mathcal{M}_{\mathcal{T}^{\mathrm{s}}_{u,k}(\mu)}(1+\theta)+(1-\lambda)\right.$$
$$\left.\times\mathcal{M}_{\mathcal{S}_{u,k}(\mu)}(1-\theta)\right\} \quad (102)$$

subject to the constraints $C1''$, $C2$, $C7$, $C9$, and $C10$ given in Eqs. (85), (56), (61), (63), and (64), respectively. Specifically, weight λ and $(1-\lambda)$ represent the relative importance of the two objective functions in Eq. (102). When $\lambda = 1$, the weighted sum optimization problem $\mathbf{P_7}$ reduces to the peak AoI violation probability minimization problem, which is the same problem that we discussed in Section IV, while when $\lambda = 0$, $\mathbf{P_7}$ is simplified into the ϵ-effective capacity maximization problem. We can show that if there exists the unique optimal solution, denoted by $\boldsymbol{\mathcal{P}}^{\mathrm{opt}}$, of the weighted sum optimization problem $\mathbf{P_7}$ given by Eq. (102), then $\boldsymbol{\mathcal{P}}^{\mathrm{opt}}$ is also the Pareto optimal for the original MOP $\mathbf{P_6}$ given by Eq. (100).

Third, we need to analyze the convexity of $\mathcal{M}_{\mathcal{S}_{u,k}(\mu)}(1-\theta)$ with respect in $\boldsymbol{\mathcal{P}}$, which is equivalent to analyze the convexity of $\mathcal{M}_{\mathcal{S}_{u,k}(\mu)}(1-\theta)$ in $\gamma_{u,k}^{(\mu)}$. Using Eq. (101), we can obtain the second-order derivative of $\mathcal{M}_{\mathcal{S}_{u,k}(\mu)}(1-\theta)$ with respect to the SNR $\gamma_{u,k}^{(\mu)}$ as follows:

$$\frac{\partial^2 \mathcal{M}_{\mathcal{S}_{u,k}(\mu)}(1-\theta)}{\partial \left[\gamma_{u,k}^{(\mu)}\right]^2} = \frac{\partial^2 \mathcal{M}_{\mathcal{S}_{u,k}(\mu)}(1-\theta)}{\partial \left[\epsilon\left(\gamma_{u,k}^{(\mu)}\right)\right]^2}\left[\frac{\partial \epsilon\left(\gamma_{u,k}^{(\mu)}\right)}{\partial \gamma_{u,k}^{(\mu)}}\right]^2$$
$$+\frac{\partial \mathcal{M}_{\mathcal{S}_{u,k}(\mu)}(1-\theta)}{\partial \epsilon\left(\gamma_{u,k}^{(\mu)}\right)}\frac{\partial^2 \epsilon\left(\gamma_{u,k}^{(\mu)}\right)}{\partial \left[\gamma_{u,k}^{(\mu)}\right]^2}$$
$$\overset{(a)}{=} \left(1-e^{-\theta\log_2 M}\right)\frac{\partial^2 \epsilon\left(\gamma_{u,k}^{(\mu)}\right)}{\partial \left[\gamma_{u,k}^{(\mu)}\right]^2} \overset{(b)}{>} 0$$
$$(103)$$

where (a) is due to $\frac{\partial^2 \mathcal{M}_{\mathcal{S}_{u,k}(\mu)}(1-\theta)}{\partial \left[\epsilon\left(\gamma_{u,k}^{(\mu)}\right)\right]^2} = 0$ and (b) is due to Eq. (77). This implies that the second term $(1-\lambda)\mathcal{M}_{\mathcal{S}_{u,k}(\mu)}(1-\theta)$ of Eq. (102) is convex in $\gamma_{u,k}^{(\mu)}$. Therefore, we can observe that the objective function in problem $\mathbf{P_7}$ given by Eq. (102) subject to the constraints $C1''$, $C2$, $C9$, and $C10$ given in Eqs. (85), (56), (63), and (64), is convex in the transmit power $\boldsymbol{\mathcal{P}}$, implying that there exists a unique optimal solution to the minimization problem $\mathbf{P_7}$. Therefore, similar to the peak AoI minimization problem discussed in Section IV, the minimization problem $\mathbf{P_7}$ is a mixed integer disciplined convex program problem and can be efficiently solved by using the CVX toolbox.

2) The Optimal UAV Trajectory Policy: Similar to Section IV, once the optimal power allocation and user association policy is selected in the previous step, the minimization problem $\mathbf{P_4}$ specified by Eq. (98) becomes a feasible optimization problem in $\boldsymbol{Q}$. We can convert the joint optimization problem $\mathbf{P_4}$ given by Eq. (98) into the following MOP $\mathbf{P_8}$:

$$\mathbf{P_8}: \arg\min_{\boldsymbol{Q}} \left\{\sum_{u=1}^{U}\sum_{\mu=1}^{N}\sum_{k=1}^{K}e^{-\frac{\theta A_{\mathrm{th}}}{n}}\mathcal{M}_{\mathcal{T}^{\mathrm{I}}_{u,k}(\mu-1,\mu)}(1+\theta)\right.$$
$$\left.\times\frac{\mathcal{M}_{\mathcal{T}^{\mathrm{s}}_{u,k}(\mu)}(1+\theta)}{1-\mathcal{M}_{\mathcal{T}^{\mathrm{I}}_{u,k}(\mu-1,\mu)}(1-\theta)\mathcal{M}_{\mathcal{T}^{\mathrm{s}}_{u,k}(\mu)}(1+\theta)}\right\} \text{ and}$$
$$\arg\min_{\boldsymbol{Q}} \left\{\sum_{u=1}^{U}\sum_{\mu=1}^{N}\sum_{k=1}^{K}\mathcal{M}_{\mathcal{S}_{u,k}(\mu)}(1-\theta)\right\} \quad (104)$$

subject to the constraints $C1''$ and $C3-C10$ given in Eqs. (85) and (57)-(64), respectively. Then, we can then convert the joint optimization problem $\mathbf{P_8}$ into the following weighted

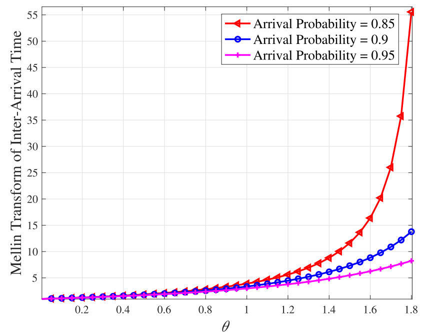

Fig. 3. The Mellin transform of the inter-arrival time $\mathcal{M}_{\mathcal{T}^{\mathrm{I}}_{u,k}(\mu-1,\mu)}(1+\theta)$ vs. θ for our proposed AoI-driven UAV schemes using FBC.

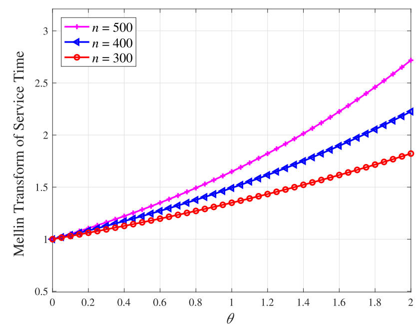

Fig. 4. The Mellin transform of the service time $\mathcal{M}_{\mathcal{T}^{\mathrm{S}}_{u,k}(\mu)}(1+\theta)$ vs. θ for our proposed AoI-driven UAV schemes using FBC.

sum optimization problem $\mathbf{P_9}$:

$$\mathbf{P_9}: \arg\min_{\boldsymbol{Q}}\Bigg\{\sum_{u=1}^{U}\sum_{\mu=1}^{N}\sum_{k=1}^{K}\widetilde{\lambda}e^{-\frac{\theta A_{\mathrm{th}}}{n}}\mathcal{M}_{\mathcal{T}^{\mathrm{I}}_{u,k}(\mu-1,\mu)}(1+\theta) \times\frac{\mathcal{M}_{\mathcal{T}^{\mathrm{S}}_{u,k}(\mu)}(1+\theta)}{1-\mathcal{M}_{\mathcal{T}^{\mathrm{I}}_{u,k}(\mu-1,\mu)}(1-\theta)\mathcal{M}_{\mathcal{T}^{\mathrm{S}}_{u,k}(\mu)}(1+\theta)} +(1-\widetilde{\lambda})\mathcal{M}_{\mathcal{S}_{u,k}(\mu)}(1-\theta)\Bigg\} \tag{105}$$

subject to the constraints $C1''$ and $C3-C10$ given in Eqs. (85) and (57)-(64), where $\widetilde{\lambda}\in[0,1]$ is the importance weight. Since we have shown that the Mellin transform of the service process $\mathcal{M}_{\mathcal{S}_{u,k}(\mu)}(1-\theta)$ in the exponential domain is convex with respect to the SNR, $\mathcal{M}_{\mathcal{S}_{u,k}(\mu)}(1-\theta)$ is also convex in $\boldsymbol{q}_{u,k}(\mu)$. In addition, since we have shown that the Mellin transform of the inter-arrival time and service time in the exponential domain are both convex with respect to $\boldsymbol{q}_{u,k}(\mu)$ as detailed in Section IV, the objective function in $\mathbf{P_9}$ specified by Eq. (105) subject to the constraints $C1''$ and $C3-C10$ given in Eqs. (85) and (57)-(64), respectively, is convex with respect to the UAV trajectory $\boldsymbol{q}_{u,k}(\mu)$. This implies that there exits a unique optimal solution to the weighted sum optimization problem $\mathbf{P_9}$, i.e., there exits the Pareto optimal for the original MOP problem $\mathbf{P_8}$ given by Eq. (104). Therefore, the minimization problem $\mathbf{P_9}$ can be quickly and efficiently solved by using the same approach as detailed in Section IV.

VI. Performance Evaluations

We use MATLAB-based simulations to validate and evaluate our proposed AoI-driven UAV multimedia mobile networks under statistical delay and error-rate bounded QoS provisioning in the finite blocklength regime. Consider that mobile devices are randomly and uniformly distributed in a region with a radius of 1 km. Throughout our simulations, we set the number of mobile devices $K\in[100,700]$, the number of UAVs $U=15$, the maximum height of the UAV $H_{\max}$ = 100 m, the minimum height of the UAV $H_{\min}$ = 25 m, the maximum UAV velocity $V_{\max}$ = 20 m/s, the packet size of each status-update information $M\in[300,1000]$ bits, the unit time for each channel use $T=\frac{1}{M}$, the sensing performance parameter $\xi=0.01$, the successful arrival probability threshold $p_{\mathrm{th}}\in[0.8,0.9]$, and the blocklength $n\in[100,600]$.

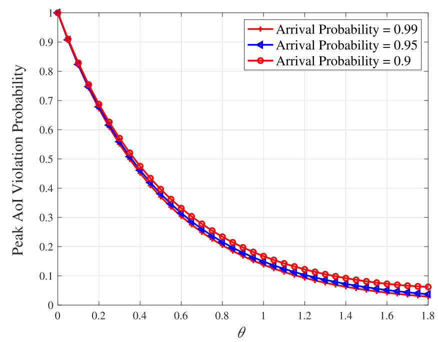

Fig. 5. The upper-bounded peak AoI violation probability vs. θ for our proposed AoI-driven UAV schemes in the finite blocklength regime.

Using Eq. (52), Fig. 3 plots the Mellin transform of the inter-arrival time $\mathcal{M}_{\mathcal{T}^{\mathrm{I}}_{u,k}(\mu-1,\mu)}(1+\theta)$ in the exponential domain as a function of θ for our proposed AoI-driven UAV schemes using FBC. Fig. 3 shows that the Mellin transform of the inter-arrival time $\mathcal{M}_{\mathcal{T}^{\mathrm{I}}_{u,k}(\mu-1,\mu)}(1+\theta)$ decreases as the arrival probability $p_{u,k}(\mu)$ increases. As shown in Fig. 3, the Mellin transform of the inter-arrival time $\mathcal{M}_{\mathcal{T}^{\mathrm{I}}_{u,k}(\mu-1,\mu)}(1+\theta)$ increases as θ increases. This implies that a smaller θ ($\theta\to 0$) and a larger θ ($\theta\to\infty$) set a lower bound and upper bound on the Mellin transform of the inter-arrival time $\mathcal{M}_{\mathcal{T}^{\mathrm{I}}_{u,k}(\mu-1,\mu)}(1+\theta)$, respectively. In addition, Fig. 4 depicts the Mellin transform of the service time $\mathcal{M}_{\mathcal{T}^{\mathrm{S}}_{u,k}(\mu)}(1+\theta)$ in the exponential domain as a function of θ for our proposed AoI-driven UAV schemes in the finite blocklength regime. As shown in Fig. 4, the Mellin transform of the service time $\mathcal{M}_{\mathcal{T}^{\mathrm{S}}_{u,k}(\mu)}(1+\theta)$ increases as θ increases, which implies that a smaller θ ($\theta\to 0$) and a larger θ ($\theta\to\infty$) lead to a lower bound and upper bound on the Mellin transform of the service time $\mathcal{M}_{\mathcal{T}^{\mathrm{S}}_{u,k}(\mu)}(1+\theta)$, respectively.

Setting the SNR $\gamma_{u,k}^{(\mu)}=5$ dB, blocklength $n=300$, and the peak AoI threshold $A_{\mathrm{th}}=50$, Fig. 5 plots the upper-bounded peak AoI violation probability as a function of θ for our proposed AoI-driven UAV schemes in the finite blocklength regime. Fig. 5 shows that the upper-bounded peak AoI violation probability decreases as θ increases. We can also observe from Fig. 5 that with a larger arrival probability $p_{u,k}(\mu)$ at the UAV, we can achieve a smaller value of the upper-bounded peak AoI violation probability.

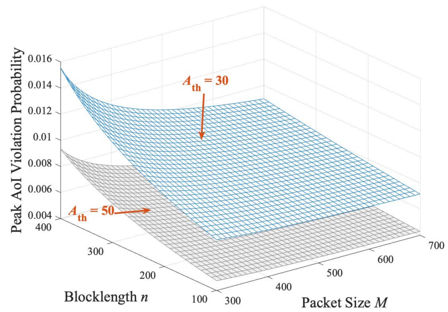

Fig. 6. The upper-bounded peak AoI violation probability function $\epsilon_{u,k}^{(\mu,\mathrm{AoI})}$ vs. blocklength n and packet size M for our proposed schemes using FBC.

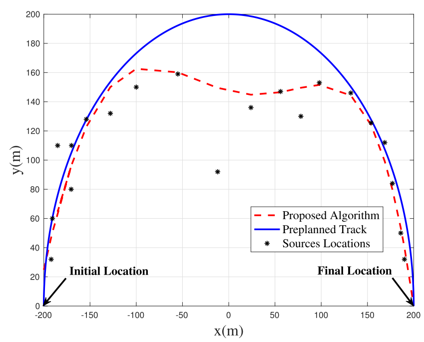

Fig. 7. The proposed UAV trajectory algorithm and preplanned trajectory for our proposed schemes.

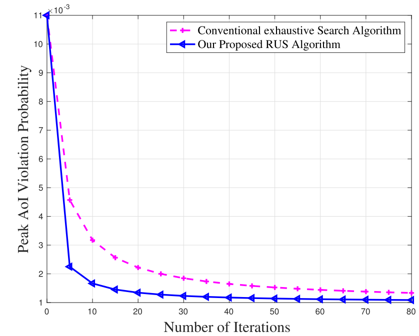

Fig. 8. The convergence of our proposed RUS based optimization algorithm.

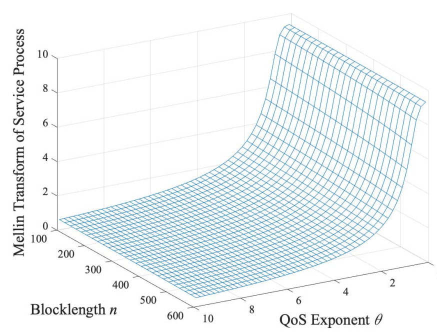

Fig. 9. The Mellin transform of the service process $\mathcal{M}_{\mathcal{S}_{u,k}(\mu)}(1-\theta)$ vs. blocklength n and θ for our proposed AoI-driven UAV schemes using FBC.

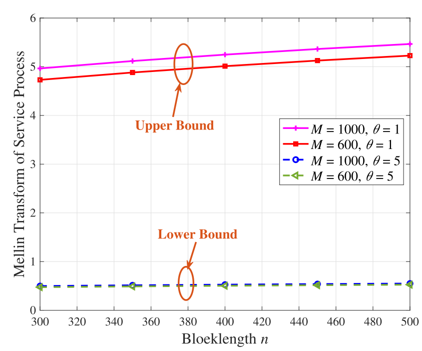

Fig. 10. The Mellin transform of the service process $\mathcal{M}_{\mathcal{S}_{u,k}(\mu)}(1-\theta)$ vs. the blocklength n for our proposed AoI-driven UAV schemes using FBC.

We set the SNR $\gamma_{u,k}^{(\mu)} = 5$ dB, the arrival probability $p_{u,k}(\mu) = 0.99$, and the peak AoI threshold $A_{\mathrm{th}} = \{30, 50\}$. Fig. 6 depicts the peak AoI violation probability $\epsilon_{u,k}^{(\mu,\mathrm{AoI})}$ as a function of both blocklength n and status-update data packet size M for our proposed schemes using FBC. Fig. 6 shows that the peak AoI violation probability $\epsilon_{u,k}^{(\mu,\mathrm{AoI})}$ increases with the blocklength n and decreases with the packet size M, respectively. We can observe from Fig. 6 that the the peak AoI violation probability $\epsilon_{u,k}^{(\mu,\mathrm{AoI})}$ is a decreasing function of the peak AoI threshold A_{th}. This implies that when the peak AoI threshold A_{th} is loose, i.e., A_{th} is large, we can achieve a smaller value of the peak AoI violation probability for our proposed AoI-driven UAV schemes.

Setting the number of mobile devices $K = 20$, Fig. 7 plots the UAV trajectories calculated by our proposed RUS based algorithm and the preplanned trajectory for one UAV. Fig. 7 shows that our proposed algorithm has more degrees of freedom by modifying the trajectory of the UAV to be close to mobile devices in order to enhance the channel gain and the total throughput.

As compared with the exhaustive search method, Fig. 8 shows the convergence of our proposed RUS based optimization algorithm with randomly generated initial points, where the terminating threshold of our proposed RUS based optimization algorithm is set as $\tau = 10^{-2}$. Fig. 8 shows that our proposed RUS Based algorithm monotonically converges. Furthermore, Fig. 8 also shows that our proposed RUS Based algorithm converges faster than the conventional exhaustive search algorithm.

Setting the status-update data packet size $M = 1000$ bits, Fig. 9 plots the Mellin transform of the service process $\mathcal{M}_{\mathcal{S}_{u,k}(\mu)}(1-\theta)$ in the exponential domain with varying blocklengths n and θ for our proposed schemes using FBC. Fig. 9 shows that when $\theta \to \infty$, the Mellin transform of the service process $\mathcal{M}_{\mathcal{S}_{u,k}(\mu)}(1-\theta)$ goes to zero. In addition, setting the blocklength $n = 300$ and $\theta \in \{1, 5\}$, Fig. 10 depicts the Mellin transform of the service process $\mathcal{M}_{\mathcal{S}_{u,k}(\mu)}(1-\theta)$ in the exponential domain as a function of the blocklength n in the finite blocklength regime. As shown in Fig. 10, the Mellin transform of the service process $\mathcal{M}_{\mathcal{S}_{u,k}(\mu)}(1-\theta)$ is an increasing function of the blocklength n. We can observe from Fig. 9 and Fig. 10 that a smaller θ ($\theta \to 0$) and a larger

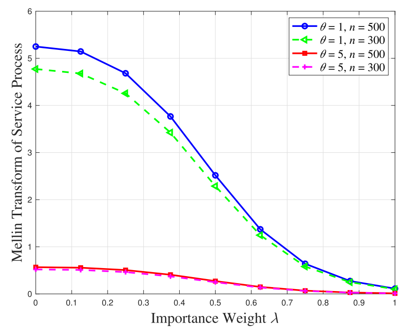

Fig. 11. The Mellin transform of the service process $\mathcal{M}_{\mathcal{S}_{u,k}(\mu)}(1-\theta)$ vs. the important weight λ for our proposed AoI-driven UAV schemes using FBC.

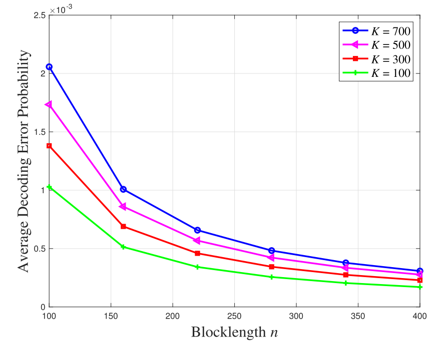

Fig. 13. The average decoding error probability vs. the number of mobile devices K for our proposed FBC based AoI-driven UAV schemes.

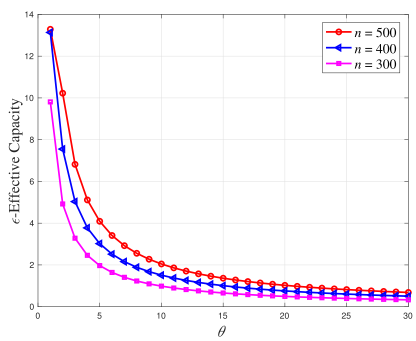

Fig. 12. The ϵ-effective capacity vs. θ for our proposed FBC based AoI-driven UAV schemes.

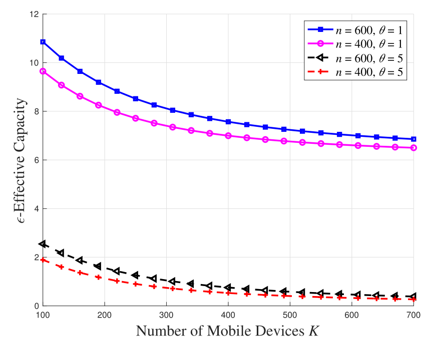

Fig. 14. The ϵ-effective capacity vs. the number of mobile devices K for our proposed FBC based AoI-driven UAV schemes.

θ ($\theta \to \infty$) set an upper bound and lower bound on the Mellin transform of the service process $\mathcal{M}_{\mathcal{S}_{u,k}(\mu)}(1-\theta)$, respectively.

Setting the blocklength $n \in \{300, 500\}$ and $\theta \in \{1, 5\}$, Fig. 11 plots the Mellin transform of the service process $\mathcal{M}_{\mathcal{S}_{u,k}(\mu)}(1-\theta)$ in the exponential domain as a function of the important weight λ for our proposed schemes. As shown in Fig. 11, the Mellin transform of the service process $\mathcal{M}_{\mathcal{S}_{u,k}(\mu)}(1-\theta)$ is a decreasing function of λ. This happens because the increase of the important weight λ raises the priority of the Mellin transform of the service time $\mathcal{M}_{\mathcal{T}^{\mathrm{S}}_{u,k}(\mu)}(1+\theta)$, i.e., the peak AoI violation probability, and diminishes the importance of the Mellin transform of the service process $\mathcal{M}_{\mathcal{S}_{u,k}(\mu)}(1-\theta)$, i.e., the ϵ-effective capacity.

Furthermore, setting the SNR $\gamma_{u,k}^{(\mu)} = 5$ dB and the status-update data packet size $M = 1000$ bits, Fig. 12 plots the ϵ-effective capacity as a function of θ for our proposed AoI-driven UAV schemes in the finite blocklength regime. We can observe from Fig. 12 that the ϵ-effective capacity increases with the blocklength n. Fig. 12 also shows that the ϵ-effective capacity is a decreasing function in terms of θ. This implies that a smaller θ ($\theta \to 0$) and a larger θ ($\theta \to \infty$) lead to an upper bound and lower bound on the ϵ-effective capacity, respectively.

We set the SNR $\gamma_{u,k}^{(\mu)} = 5$ dB and the peak AoI threshold $A_{\text{th}} = 50$. Considering different numbers of mobile devices K, Fig. 13 depicts the average decoding error probability as a function of the blocklength n for our proposed schemes using FBC. Fig. 13 shows that the average decoding error probability increases as the blocklength n increases. We can observe from Fig. 13 that the performance degradation in terms of the average block error probability function with the increasing number of mobile users K is mild, implying the remarkable potential as well as the strong and robust scalability in supporting *massive access* by vast mobile devices for our proposed schemes. Fig. 14 plots the ϵ-effective capacity as a function of the number of mobile devices K for our proposed AoI-driven UAV schemes in the finite blocklength regime. We can also observe from Fig. 14 that the ϵ-effective capacity increases as the number of mobile devices K and will finally converge to a certain value, which implies the potential to support *massive* number of mobile users.

VII. Conclusion

We have proposed AoI-driven statistical delay and error-rate bounded QoS provisioning schemes to efficiently support mURLLC over UAV 6G multimedia mobile networks in the finite blocklength regime. In particular, we have developed UAV wireless networking models with 3D wireless channels in the finite blocklength regime. Then, we have built up AoI-metric based modeling frameworks by applying the SNC to upper bound the peak AoI violation probability in supporting mURLLC services using FBC. Taking into account the transmit power and UAV trajectory constraints, we have formulated and solved the peak AoI violation probability minimization problem in the finite blocklength regime. In addition, we have jointly optimized the peak AoI violation probability and ϵ-effective capacity and characterized their tradeoff in supporting our proposed statistical delay and error-rate bounded QoS provisioning under FBC. We have conducted a set of simulations to validate and evaluate our developed schemes in supporting statistical delay and error-rate bounded QoS provisioning.

REFERENCES

[1] X. Zhang, J. Tang, H.-H. Chen, S. Ci, and M. Guizani, "Cross-layer-based modeling for quality of service guarantees in mobile wireless networks," *IEEE Commun. Mag.*, vol. 44, no. 1, pp. 100–106, Jan. 2006.

[2] J. Tang and X. Zhang, "Quality-of-service driven power and rate adaptation over wireless links," *IEEE Trans. Wireless Commun.*, vol. 6, no. 8, pp. 3058–3068, Aug. 2007.

[3] J. Tang and X. Zhang, "Cross-layer resource allocation over wireless relay networks for quality of service provisioning," *IEEE J. Sel. Areas Commun.*, vol. 25, no. 4, pp. 645–656, May 2007.

[4] A. Burchard, J. Liebeherr, and S. D. Patek, "A min-plus calculus for end-to-end statistical service guarantees," *IEEE Trans. Inf. Theory*, vol. 52, no. 9, pp. 4105–4114, Sep. 2006.

[5] W. Saad, M. Bennis, and M. Chen, "A vision of 6G wireless systems: Applications, trends, technologies, and open research problems," *IEEE Netw.*, vol. 34, no. 3, pp. 134–142, May 2020.

[6] K. B. Letaief, W. Chen, Y. Shi, J. Zhang, and Y.-J.-A. Zhang, "The roadmap to 6G: AI empowered wireless networks," *IEEE Commun. Mag.*, vol. 57, no. 8, pp. 84–90, Aug. 2019.

[7] Z. Zhang *et al.*, "6G wireless networks: Vision, requirements, architecture, and key technologies," *IEEE Veh. Technol. Mag.*, vol. 14, no. 3, pp. 28–41, Sep. 2019.

[8] H. Su and X. Zhang, "Cross-layer based opportunistic MAC protocols for QoS provisionings over cognitive radio wireless networks," *IEEE J. Sel. Areas Commun.*, vol. 26, no. 1, pp. 118–129, Jan. 2008.

[9] X. Zhang, W. Cheng, and H. Zhang, "Heterogeneous statistical QoS provisioning over airborne mobile wireless networks," *IEEE J. Sel. Areas Commun.*, vol. 36, no. 9, pp. 2139–2152, Sep. 2018.

[10] X. Zhang, W. Cheng, and H. Zhang, "Heterogeneous statistical QoS provisioning over 5G mobile wireless networks," *IEEE Netw.*, vol. 28, no. 6, pp. 46–53, Nov. 2014.

[11] H. Ji, S. Park, J. Yeo, Y. Kim, J. Lee, and B. Shim, "Ultra-reliable and low-latency communications in 5G downlink: Physical layer aspects," *IEEE Wireless Commun.*, vol. 25, no. 3, pp. 124–130, Jun. 2018.

[12] X. Chen, D. W. K. Ng, W. Yu, E. G. Larsson, N. Al-Dhahir, and R. Schober, "Massive access for 5G and beyond," *IEEE J. Sel. Areas Commun.*, vol. 39, no. 3, pp. 615–637, Mar. 2021.

[13] M. Amjad, L. Musavian, and S. Aïssa, "NOMA versus OMA in finite blocklength regime: Link-layer rate performance," *IEEE Trans. Veh. Technol.*, vol. 69, no. 12, pp. 16253–16257, Dec. 2020.

[14] E. Yaacoub and M.-S. Alouini, "A key 6G challenge and opportunity—Connecting the base of the pyramid: A survey on rural connectivity," *Proc. IEEE*, vol. 108, no. 4, pp. 533–582, Apr. 2020.

[15] X. Zhang, J. Wang, and H. V. Poor, "Statistical delay and error-rate bounded QoS provisioning over mmWave cell-free M-MIMO and FBC-HARQ-IR based 6G wireless networks," *IEEE J. Sel. Areas Commun.*, vol. 38, no. 8, pp. 1661–1677, Aug. 2020.

[16] W. Yang, G. Durisi, T. Koch, and Y. Polyanskiy, "Quasi-static multiple-antenna fading channels at finite blocklength," *IEEE Trans. Inf. Theory*, vol. 60, no. 7, pp. 4232–4265, Jul. 2014.

[17] G. Durisi, T. Koch, and P. Popovski, "Toward massive, ultrareliable, and low-latency wireless communication with short packets," *Proc. IEEE*, vol. 104, no. 9, pp. 1711–1726, Sep. 2016.

[18] Y. Polyanskiy, H. V. Poor, and S. Verdú, "Channel coding rate in the finite blocklength regime," *IEEE Trans. Inf. Theory*, vol. 56, no. 5, pp. 2307–2359, May 2010.

[19] Y. Polyanskiy and S. Verdú, "Empirical distribution of good channel codes with nonvanishing error probability," *IEEE Trans. Inf. Theory*, vol. 60, no. 1, pp. 5–21, Jan. 2014.

[20] Y. Polyanskiy, H. V. Poor, and S. Verdú, "Feedback in the non-asymptotic regime," *IEEE Trans. Inf. Theory*, vol. 57, no. 8, pp. 4903–4925, Aug. 2011.

[21] B. Li, Z. Fei, and Y. Zhang, "UAV communications for 5G and beyond: Recent advances and future trends," *IEEE Internet Things J.*, vol. 6, no. 2, pp. 2241–2263, Apr. 2019.

[22] Y. Sun, D. Xu, D. W. K. Ng, L. Dai, and R. Schober, "Optimal 3D-trajectory design and resource allocation for solar-powered UAV communication systems," *IEEE Trans. Commun.*, vol. 67, no. 6, pp. 4281–4298, Jun. 2019.

[23] H. Ren, C. Pan, K. Wang, Y. Deng, M. Elkashlan, and A. Nallanathan, "Achievable data rate for URLLC-enabled UAV systems with 3-D channel model," *IEEE Wireless Commun. Lett.*, vol. 8, no. 6, pp. 1587–1590, Dec. 2019.

[24] C. She, C. Liu, T. Q. S. Quek, C. Yang, and Y. Li, "UAV-assisted uplink transmission for ultra-reliable and low-latency communications," in *Proc. IEEE Int. Conf. Commun. Workshops (ICC Workshops)*, May 2018, pp. 1–6.

[25] M. Ozger, M. Vondra, and C. Cavdar, "Towards beyond visual line of sight piloting of UAVs with ultra reliable low latency communication," in *Proc. IEEE Global Commun. Conf. (GLOBECOM)*, Dec. 2018, pp. 1–6.

[26] C. Pan, H. Ren, Y. Deng, M. Elkashlan, and A. Nallanathan, "Joint blocklength and location optimization for URLLC-enabled UAV relay systems," *IEEE Commun. Lett.*, vol. 23, no. 3, pp. 498–501, Mar. 2019.

[27] C. She, C. Liu, T. Q. S. Quek, C. Yang, and Y. Li, "Ultra-reliable and low-latency communications in unmanned aerial vehicle communication systems," *IEEE Trans. Commun.*, vol. 67, no. 5, pp. 3768–3781, May 2019.

[28] H. Ren, C. Pan, K. Wang, W. Xu, M. Elkashlan, and A. Nallanathan, "Joint transmit power and placement optimization for URLLC-enabled UAV relay systems," *IEEE Trans. Veh. Technol.*, vol. 69, no. 7, pp. 8003–8007, Jul. 2020.

[29] K. Wang, C. Pan, H. Ren, W. Xu, L. Zhang, and A. Nallanathan, "Packet error probability and effective throughput for ultra-reliable and low-latency UAV communications," *IEEE Trans. Commun.*, vol. 69, no. 1, pp. 73–84, Jan. 2021.

[30] S. Kaul, R. Yates, and M. Gruteser, "Real-time status: How often should one update?" in *Proc. IEEE INFOCOM*, Mar. 2012, pp. 2731–2735.

[31] Y. Sun, E. Uysal-Biyikoglu, R. D. Yates, C. E. Koksal, and N. B. Shroff, "Update or wait: How to keep your data fresh," *IEEE Trans. Inf. Theory*, vol. 63, no. 11, pp. 7492–7508, Nov. 2017.

[32] M. Costa, M. Codreanu, and A. Ephremides, "On the age of information in status update systems with packet management," *IEEE Trans. Inf. Theory*, vol. 62, no. 4, pp. 1897–1910, Apr. 2016.

[33] J. Liu, X. Wang, B. Bai, and H. Dai, "Age-optimal trajectory planning for UAV-assisted data collection," in *Proc. IEEE Conf. Comput. Commun. Workshops (INFOCOM WKSHPS)*, Apr. 2018, pp. 553–558.

[34] M. A. Abd-Elmagid and H. S. Dhillon, "Average peak age-of-information minimization in UAV-assisted IoT networks," *IEEE Trans. Veh. Technol.*, vol. 68, no. 2, pp. 2003–2008, Feb. 2019.

[35] S. Zhang, H. Zhang, Z. Han, H. V. Poor, and L. Song, "Age of information in a cellular Internet of UAVs: Sensing and communication trade-off design," *IEEE Trans. Wireless Commun.*, vol. 19, no. 10, pp. 6578–6592, Oct. 2020.

[36] X. Chen and S. S. Bidokhti, "Benefits of coding on age of information in broadcast networks," in *Proc. IEEE Inf. Theory Workshop (ITW)*, Aug. 2019, pp. 1–5.

[37] A. Al-Hourani, S. Kandeepan, and S. Lardner, "Optimal LAP altitude for maximum coverage," *IEEE Wireless Commun. Lett.*, vol. 3, no. 6, pp. 569–572, Dec. 2014.

[38] V. V. Shakhov and I. Koo, "Experiment design for parameter estimation in probabilistic sensing models," *IEEE Sensors J.*, vol. 17, no. 24, pp. 8431–8437, Dec. 2017.

[39] J. Hu, H. Zhang, and L. Song, "Reinforcement learning for decentralized trajectory design in cellular UAV networks with sense-and-send protocol," *IEEE Internet Things J.*, vol. 6, no. 4, pp. 6177–6189, Aug. 2019.

[40] C.-S. Chang, *Performance Guarantees in Communication Networks*. London, U.K.: Springer-Verlag, 2012.

[41] H. Al-Zubaidy, J. Liebeherr, and A. Burchard, "Network-layer performance analysis of multihop fading channels," *IEEE/ACM Trans. Netw.*, vol. 24, no. 1, pp. 204–217, Feb. 2016.

[42] M. Fidler, B. Walker, and Y. Jiang, "Non-asymptotic delay bounds for multi-server systems with synchronization constraints," *IEEE Trans. Parallel Distrib. Syst.*, vol. 29, no. 7, pp. 1545–1559, Jul. 2018.

[43] M. Grant and S. Boyd. (Mar. 2014). *CVX: MATLAB Software for Disciplined Convex Programming, Version 2.1*. [Online]. Available: http://cvxr.com/cvx

[44] T. Ye, H. T. Kaur, S. Kalyanaraman, and M. Yuksel, "Large-scale network parameter configuration using an on-line simulation framework," *IEEE/ACM Trans. Netw.*, vol. 16, no. 4, pp. 777–790, Aug. 2008.

[45] C.-S. Chang, "Stability, queue length, and delay of deterministic and stochastic queueing networks," *IEEE Trans. Autom. Control*, vol. 39, no. 5, pp. 913–931, May 1994.

[46] K. Deb, "Multi-objective optimization," in *Search Methodologies*. Boston, MA, USA: Springer, 2014, pp. 403–449.

[47] L. Zheng and C. W. Tan, "Maximizing sum rates in cognitive radio networks: Convex relaxation and global optimization algorithms," *IEEE J. Sel. Areas Commun.*, vol. 32, no. 3, pp. 667–680, Mar. 2014.

Xi Zhang (Fellow, IEEE) received the B.S. and M.S. degrees from Xidian University, Xi'an, China, the M.S. degree from Lehigh University, Bethlehem, PA, USA, all in electrical engineering and computer science, and the Ph.D. degree in electrical engineering and computer science (Electrical Engineering-Systems) from the University of Michigan, Ann Arbor, MI, USA.

He is currently a Full Professor and the Founding Director of the Networking and Information Systems Laboratory, Department of Electrical and Computer Engineering, Texas A&M University, College Station. He is a fellow of the IEEE for contributions to quality of service (QoS) theory in mobile wireless networks. He was with the Networks and Distributed Systems Research Department, AT&T Bell Laboratories, Murray Hill, NJ, USA, and AT&T Laboratories Research, Florham Park, NJ, in 1997. He was a Research Fellow with the School of Electrical Engineering, University of Technology, Sydney, Australia, and the Department of Electrical and Computer Engineering, James Cook University, Australia. He has published more than 400 research articles on wireless networks and communications systems, network protocol design and modeling, statistical communications, random signal processing, information theory, and control theory and systems. He is an IEEE Distinguished Lecturer of the IEEE Communications Society and the IEEE Vehicular Technology Society. He received the TEES Select Young Faculty Award for Excellence in Research Performance from the Dwight Look College of Engineering at Texas A&M University, College Station, in 2006, and the Outstanding Faculty Award from Department of Electrical and Computer Engineering, Texas A&M University, in 2020. He received the U.S. National Science Foundation CAREER Award in 2004 for his research in the areas of mobile wireless and multicast networking and systems. He received the six best paper awards at IEEE GLOBECOM 2020, IEEE ICC 2018, IEEE GLOBECOM 2014, IEEE GLOBECOM 2009, IEEE GLOBECOM 2007, and IEEE WCNC 2010, respectively. One of his IEEE JOURNAL ON SELECTED AREAS IN COMMUNICATIONS papers has been listed as the IEEE Best Readings Paper (receiving the highest citation rate among all IEEE TRANSACTIONS/Journal articles in the area) on wireless cognitive radio networks and statistical QoS provisioning over mobile wireless networking.

Prof. Zhang is serving or has served as an Editor for IEEE TRANSACTIONS ON COMMUNICATIONS, IEEE TRANSACTIONS ON WIRELESS COMMUNICATIONS, IEEE TRANSACTIONS ON VEHICULAR TECHNOLOGY, IEEE TRANSACTIONS ON GREEN COMMUNICATIONS AND NETWORKING, and IEEE TRANSACTIONS ON NETWORK SCIENCE AND ENGINEERING. He served twice as a Guest Editor for IEEE JOURNAL ON SELECTED AREAS IN COMMUNICATIONS for Special Issue on "Broadband Wireless Communications for High Speed Vehicles" and Special Issue on "Wireless Video Transmissions." He was an Associate Editor for IEEE COMMUNICATIONS LETTERS. He served twice as the Lead Guest Editor for *IEEE Communications Magazine* for Special Issue on "Advances in Cooperative Wireless Networking" and Special Issue on "Underwater Wireless Communications and Networks: Theory and Applications." He served as a Guest Editor for *IEEE Wireless Communications Magazine* for Special Issue on "Next Generation CDMA vs. OFDMA for 4G Wireless Applications." He served as an Editor for *Wireless Communications and Mobile Computing* (Wiley), *Journal of Computer Systems, Networks, and Communications*, and *Security and Communication Networks* (Wiley). He served as an Area Editor for *Computer Communications* (Elsevier), and among many others. He is serving or has served as the TPC Chair for IEEE GLOBECOM 2011, the TPC Vice-Chair for IEEE INFOCOM 2010, the TPC Area Chair for IEEE INFOCOM 2012, the Panel/Demo/Poster Chair for ACM MobiCom 2011, the General Chair for IEEE WCNC 2013, and the TPC Chair for IEEE INFOCOM 2017–2019 Workshops on "Integrating Edge Computing, Caching, and Offloading in Next Generation Networks."

Jingqing Wang received the B.S. degree in electronics and information engineering from Northwestern Polytechnical University, Xi'an, China. She is currently pursuing the Ph.D. degree with the Networking and Information Systems Laboratory, Department of Electrical and Computer Engineering, Texas A&M University, College Station, TX, USA, under the supervision of Professor Xi Zhang. Her research interests focus on big data based 5G and beyond mobile wireless networks technologies, statistical delay and error-rate bounded QoS provisioning, 6G mURLLC, information-theoretic analyses of FBC, and emerging machine learning techniques over 5G and beyond mobile wireless networks. She won the Best Paper Award from the IEEE GLOBECOM in 2020 and 2014, respectively, the Hagler Institute for Advanced Study Heep Graduate Fellowship Award from Texas A&M University in 2018, and the Dr. R. K. Pandey and Christa U. Pandey'84 Fellowship, Texas A&M University, USA, for the period 2020–2021.

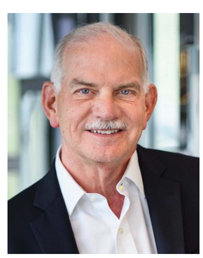

H. Vincent Poor (Life Fellow, IEEE) received the Ph.D. degree in EECS from Princeton University in 1977, and the D.Eng. degree (Hons.) from the University of Waterloo in 2019.

From 1977 to 1990, he was with the Faculty of the University of Illinois at Urbana-Champaign. Since 1990, he has been with the Faculty at Princeton, where he is currently the Michael Henry Strater University Professor. From 2006 to 2016, he served as the Dean of the Princeton's School of Engineering and Applied Science. He has held visiting appointments at several other universities, including most recently at Berkeley and Cambridge. His research interests are in the areas of information theory, machine learning and network science, and their applications in wireless networks, energy systems, and related fields. Among his publications in these areas is the forthcoming book *Machine Learning and Wireless Communications* (Cambridge University Press, 2021). He is a member of the National Academy of Engineering and the National Academy of Sciences. He is a Foreign Member of the Chinese Academy of Sciences, the Royal Society, and other national and international academies. His work received the 2017 IEEE Alexander Graham Bell Medal.